AES 8211352
Final Report

APTECH engineering services, inc ENGINEERING CONSULTANTS

795 SAN ANTONIO ROAD • PALO ALTO • CALIFORNIA 94303 (415) 858 • 2863

ANALYSIS OF INACCESSIBLE AND POTENTIALLY REJECTABLE DEFECTS IN PERRY NUCLEAR POWER PLANT

Prepared by

Warren P. McNaughton
Geoffrey R. Egan
Jeffrey D. Byron

Aptech Engineering Services, Inc
795 San Antonio Road
Palo Alto, California 94303

Prepared for

Gilbert Associates, Inc.
Post Office Box 1498
Reading, Pennsylvania 19603

Attention: Paul B. Gudikunst

May 1983

QUALITY ASSURANCE VERIFICATION RECORD SHEET

Title: Analysis of Inaccessible and Potentially Rejectable Defects in Perry Nuclear Power Plant

Originated by: Warren P. McNaughton 5-25-83

Warren P. McNaughton

Jeffrey D. Byron 5-26-83

Jeffrey D. Byron

Verified by: Jeffrey L. Grover 26 MAY 83

Jeffrey L. Grover

Approved by: Geoffrey R. Egan 5-26-83

Geoffrey R. Egan

Quality Assurance Approval: Russell C. Cipolla 5/26/83

Russell C. Cipolla

TABLE OF CONTENTS

TABLE OF CONTENTS
(Continued)

SYNOPSIS

This report summarizes the results of fracture mechanics and fatigue evaluations which were performed for the Perry Nuclear Power Plant Units 1 and 2. These evaluations were performed for several regions of the containment structures as follows:

- Inaccessible locations in weld joints 1-1 and 2-1 which had weld indications.
- Three inaccessible weld locations in joints 1-4, 1-7, and 1-9.

In these last three locations, incomplete radiographic information exists to establish the existing defect size (for example, whether or not full repairs were made); however, sufficient data do exist to characterize the maximum extent of a defect that could remain in the structure and this potential defect has been analyzed.

The evaluations that were performed required three types of input data. These data were stresses, both applied and weld residual stresses, flaw geometries and material properties.

Recently, revised stress data were supplied by Gilbert Associates for the containment. Bounding cyclical and steady state stresses were incorporated to provide an analysis that results in a conservative evaluation of the weld indications. A conservative residual stress determination was also made by assessing the appropriate experimental data.

Flaw data were obtained from radiographic enhancement techniques performed on supplied radiographs. These techniques were used to provide accurate

sizing of the indications. Such determinations remove some of the conservatism which has traditionally been used to assess structures with defects in the absence of actual flaw size data.

Material properties such as strength, fracture toughness and crack growth rates were determined using available Certified Material Test Reports and by comparison to generic data obtained from the open literature.

The results confirm that crack growth by fatigue is small over the design plant lifetime, even assuming conservative stress levels, bounding initial flaws and worst case crack propagation rates. Furthermore, it is shown that the applied stress intensity values reached during and after such growth are less than the critical value to cause structural failure. The conservative result of the linear elastic fracture mechanics methodology used in this work is then confirmed using both elastic-plastic and net section collapse (or limit load) methods. It is shown that relatively long and deep flaws can be tolerated even with the conservative assumptions which have been made.

Section 1
INTRODUCTION

A review of radiographs for the Perry Nuclear Power Plant Units 1 and 2, has found certain containment welds that contain potentially rejectable indications. The radiographs can be grouped into two logical regions of interest.

The first group of weld indications are found in radiographs associated with weld joints 1-1 and 2-1. These weld locations are inaccessible. They are located in the containment wall (see figure 1-1) in double sided butt welds and are covered on the inside of the containment by a doubler plate. Defects have been found that would be considered rejectable by ASME Boiler and Pressure Vessel Code criteria. Twenty-one radiographs of weld 1-1 and 43 radiographs from inaccessible regions of Unit 2 were reviewed. The stresses in Units 1 and 2 are identical. Bounding defects were developed considering both Unit 1 and Unit 2 indications.

The second group of indications consists of three specific weld locations in joints 1-4, 1-7 and 1-9. Weld joint 1-4 has a defect at location (79-80) 11-12, which has been sized at 2 3/4" long and 1/16" in height. It appears to be a plate delamination (CD-139, Attachment 4).

In weld joint 1-7, at location (110-111) 25-26, the film shows a questionable indication. If this location were accessible the disposition would be to grind and retake. In addition, the film is in question because it does not cover the full indication. At maximum, it would be a 9/16" long slag line (CD-139, Attachment 3).

In weld joint 1-9, at location (134-135) 24-25, the film has no indications, however, the adjacent film did have repair which extended into this station. A slag inclusion may still be present, maximum length equal to 1 3/4" (CD-139, Attachment 3). These locations are also inaccessible

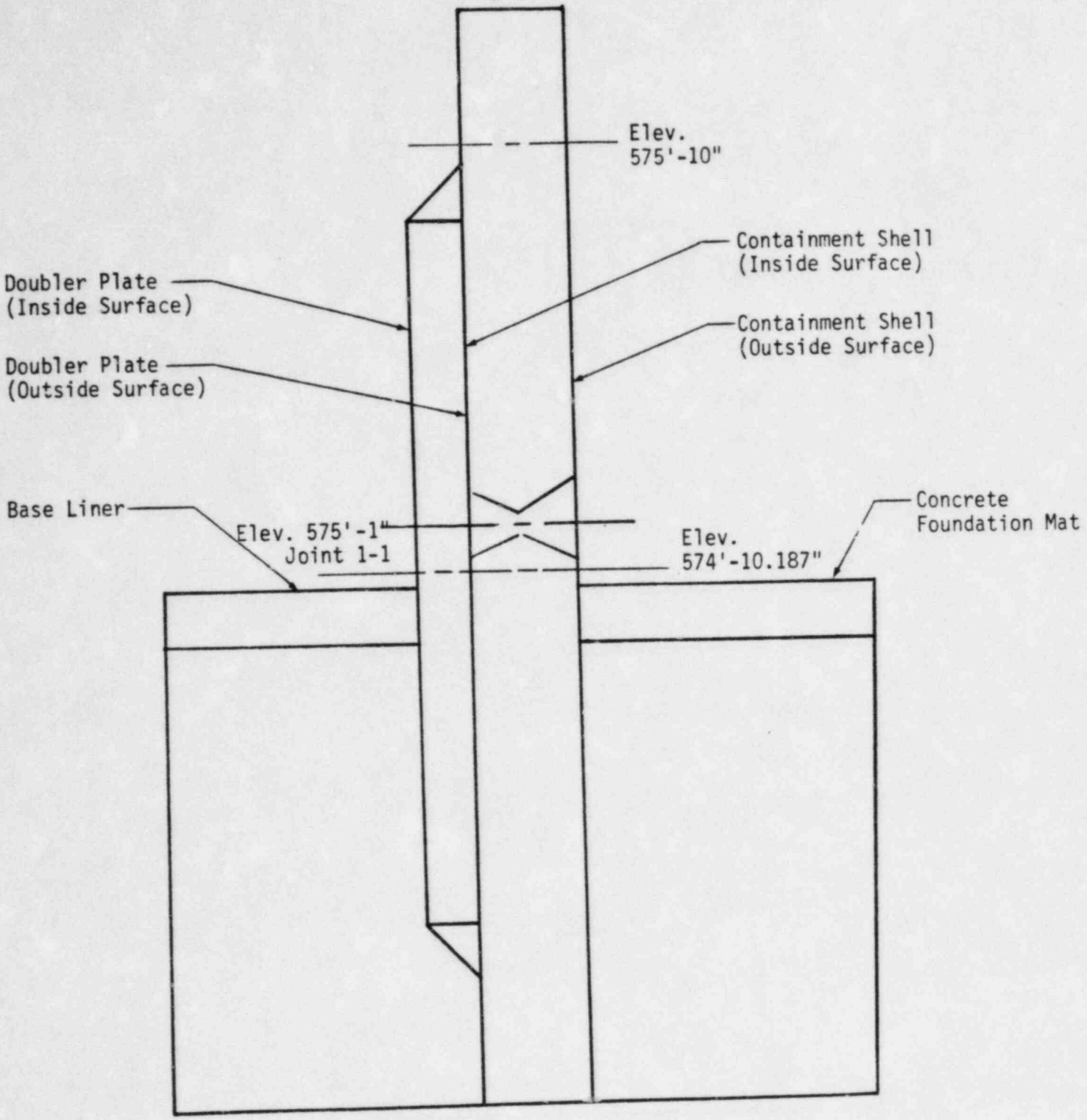

Figure 1-1 Typical Horizontal Weld Joint
(1-1 shown here)

and the existing radiographic information can be used to provide worst case estimates of defect size remaining in the structure, or of the possible incomplete repairs.

All welds have been fabricated using E7018 weld metal. The defects are completely contained in the weld metal except in joint 1-4 where the indication is in the base material-SA516 Grade 70. The concern in each case is that the indications if unrepaired, may lead to early structural failure. This report addresses that concern and does so by evaluating the potential for defect growth by a fatigue mechanism and concurrent or subsequent failure by fracture.

The remainder of this report consists of six sections. Section 2.0 outlines the analysis methods that have been used to evaluate the defects. The next four sections introduce and discuss input to the analytical model. They are: the evaluation of stresses-both applied and residual (Section 3.0), characterization of material properties (Sections 4.0 and 5.0), and results of the enhancement work performed (Section 6.0). Section 7.0 provides the results of the analysis performed. Conclusions and summary are provided in Section 8.0. Throughout the report, reference is made to documents which have been used to provide input information to the analysis. These documents which are considered controlled under the requirements of the Aptech quality assurance system are designated Controlled Document (CD) and are referenced in Appendix D of this report.

Section 1
REFERENCES

1-1 American Society of Mechanical Engineers, Boiler and Pressure Vessel Code, Section III, 1974 Edition, Winter 1975 Addenda.

Section 2
ANALYSIS METHODS

The following sections discuss those aspects of fracture mechanics and fatigue theory which were used in the analysis of the present problem. A presentation of general fracture mechanics background (2.1) is followed by a discussion of methods of analysis to assess fatigue growth (2.2).

2.1 Fracture Mechanics Background

The failure behavior of structures under monotonic (slowly increasing) loading can be classified into three regimes in which a specific type of failure mode is appropriate. These three regimes cover brittle fracture, ductile fracture and plastic collapse. The disciplines required to assess these regimes are:

- Linear Elastic Fracture Mechanics (LEFM) - The structure fails in a brittle manner and, on a macro scale, the load to failure occurs within nominally elastic loading.

- Elastic-Plastic Fracture Mechanics (EPFM) - The structure fails in a ductile manner, and significant stable crack extension by tearing may precede ultimate failure.

- Fully Plastic Instability (Limit Load Theory) - The failure event is characterized by large deflections and plastic strains associated with ultimate strength collapse.

A diagram that shows the relationship between critical or failure stress and flaw size for the three failure modes is given in Figure 2-1. The shape and position of the failure locus will depend on the fracture toughness (K_{Ic}) and strength properties (σ_ℓ) of the material, as well as the structural geometry and type of loading.

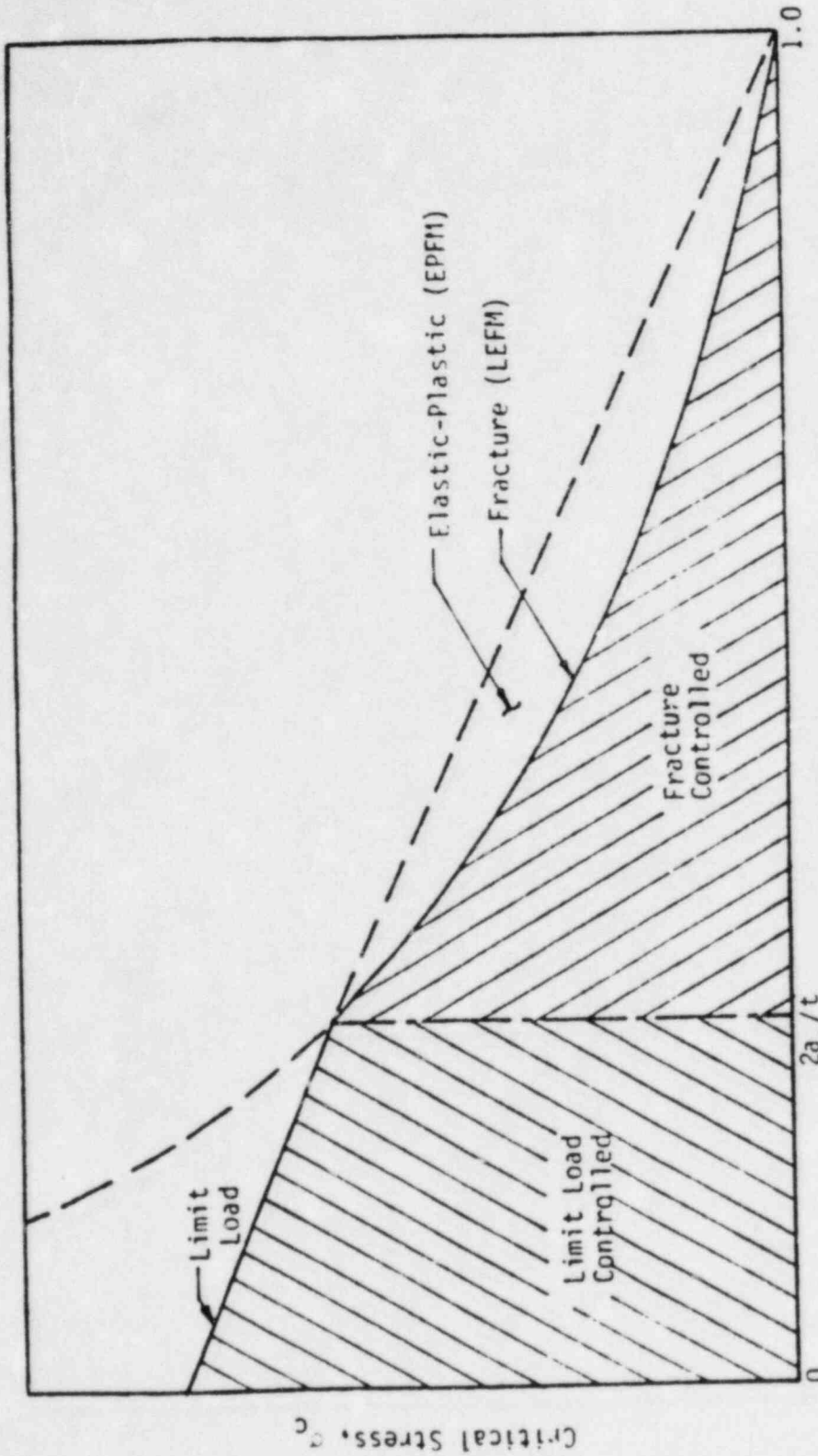

Figure 2-1 Schematic Showing the Relationship Between Failure Stress and Flaw Size For Two Limiting Failure Modes.

2.1.1 Linear Elastic Fracture Mechanics (LEFM)

The principles of linear elastic fracture mechanics (LEFM) are applied to assess quantitatively the conditions for brittle fracture. Brittle fracture consists of two separate events: (1) the initiation of a crack, and (2) the subsequent propagation of the crack to complete failure. Each of these events, initiation and subsequent propagation, has different characteristics. For ferritic structural steels of the SA516 type and carbon manganese weld metal of the E7018 class, the resistance to a propagating fracture is usually lower than the resistance to fracture initiation under slowly applied loads. This is because steels of this type are sensitive to loading rate; the high loading rates associated with a running crack lead to higher yield strength and, hence, lower values of fracture toughness. In constant load situations, therefore, continued crack propagation is expected once the fracture has initiated. For this reason, no attempt is made to evaluate the characteristics of the propagating crack after it has initiated, and the criterion of fracture initiation is used as the definition of failure in the fracture analyses.

Fracture initiation occurs at a defect when the crack driving force exceeds the material's inherent resistance to crack initiation, or fracture toughness. The crack driving force is a function of the stresses acting on the defect and the geometry of the defect. The stresses which act on the defect include both primary (applied) stresses and secondary (internal) stresses. Examples of secondary stresses are residual stresses and thermal stresses that are in equilibrium across the section. The manner in which a structure will fail will be determined by the interaction of the defect geometry, loading, and material toughness.

In linear elastic fracture mechanics, the most useful parameter for characterizing the behavior of cracks is the stress intensity factor K_I, which describes the magnitude of singular stresses ahead of a crack in a linear elastic body loaded in tension. For loading normal to the crack plane (Mode I), fracture initiation occurs when the applied stress intensity factor, K_I, equals or exceeds some critical value, which is

called the fracture toughness of the material. The applied stress intensity factor can be written in the form:

$$K_I = C\sigma\sqrt{\pi a} \qquad (2.1)$$

where σ is the acting stress, a is the characteristic flaw dimension, and C is a parameter which accounts for the flaw shape, structural geometry, and the type of loading. In general, C is a function of a and in many cases must be evaluated numerically. Fracture will occur under quasi-static loading when,

$$K_I \geq K_{Ic} \qquad (2.2)$$

(i.e., when the applied stress intensity factor equals or exceeds the static fracture toughness, K_{Ic}). This means that the occurrence of fracture is controlled by: (1) the stress level, (2) the flaw size, and (3) the fracture toughness. For small flaws, low stresses and high toughness, the applied K will not reach K_{Ic}, and fracture will not occur. These relationships are relevant for material properties determined under plane strain, linear elastic conditions.

To determine the significance of the inaccessible defects in question, it is necessary to know the material fracture toughness, acting stress level and actual distribution of defect sizes and shapes. Knowing any two of these parameters, one can solve for the third. For example, the critical flaw size to cause failure is calculated from:

$$a_c = \frac{1}{\pi C^2}\left(\frac{K_{Ic}}{\sigma_c}\right)^2 \qquad (2.3)$$

if both the toughness (K_{Ic}) and the stress level (σ_c) are known. Conversely, the critical applied stress as a function of crack depth can be computed from,

$$\sigma_c = \frac{K_{Ic}}{C\sqrt{\pi a}} \qquad (2.4)$$

Although these conditions most appropriately describe the behavior of low toughness, high strength materials where little ductility precedes fracture, the use of K_{Ic} as a toughness measure for either SA516 steel or E7018 weld metal ensures a conservative estimate of critical flaw size for brittle fracture, since no account is taken of the increased toughness which results from post-yield (transitional) behavior. Incorporating transitional behavior with more pre-fracture ductility gives increased toughness levels and decreases the susceptibility of the structure to fracture from a given sized flaw. The temperature dependence of toughness properties means that at ambient or higher temperatures, both SA516 steel and E7018 weld metal are above their lower shelf values on a fracture energy versus temperature curve. This in turn implies that the use of standard elastic fracture mechanics will be conservative. Elastic-plastic crack opening displacement (COD) concepts have been used as a check on structural integrity. Elastic-plastic fracture mechanics concepts are discussed in the next section.

2.1.2 Elastic-Plastic Fracture Mechanics (EPFM)

The basic principles of EPFM have been developed over several years (2-1, 2-2, 2-4) and one national standard exists for crack opening displacement (COD) testing (2-5). This method uses critical COD values (as measures of the material toughness) which are not available for the actual field material. A review of the literature (notably 2-6) was made to check the appropriate material characteristics.

One of the best methodologies for EPFM evaluation, the British Standards Institution published document PD6493:1980 (2-7), utilizes crack opening displacement (COD) concepts. In principle, the critical condition is reached when the applied K_I or COD (δ) reaches the resistance level of toughness necessary to cause fracture (K_{Ic} or δ_c). The COD method is completely compatible with the LEFM approach (2-8) and can be used in place

of the K_{Ic} method. For applied stresses well below yield,

$$\delta = \frac{8\varepsilon_y a}{\pi} \log_e \sec\left(\frac{\pi}{2} \frac{\sigma}{\sigma_y}\right) \qquad (2.5)$$

where δ is the developed COD; e_y and σ_y are the yield strain and yield stress of the region in which the defect is sited; σ is the applied stress; and a is the half crack length of a center-cracked plate model. It can be seen from Equation 2.5 that as σ approaches σ_y, the developed COD becomes infinite. This only occurs for the elastic-perfectly-plastic material behavior that was assumed for the development of Equation 2.5. For materials that work harden, the relationship between COD and applied strain (for stresses above yield) has been determined by analytical, numerical, and experimental methods (2-9, 2-10).

As in LEFM, once the stresses and material properties have been characterized, it is possible to determine the allowable flaw size to prevent fracture initiation. It is then possible to determine the expected margin of safety between the flaws that may be in the structure and those necessary to cause failure.

2.1.3 Limit Load Analysis

As the size of a critical flaw increases, a regime is entered in which increasing material toughness no longer can prevent initiation of a crack under monotonic loading. The initiation criterion becomes independent of toughness and now becomes a function of the strength properties of the material and the remaining ligament of material. In this regime, a limit load or plastic collapse analysis describes the governing failure mode.

For limit load analysis, the critical stress to cause failure is calculated from an interaction relation common in the analysis of steel structures. This relationship between the applied membrane load (P) and bending moment (M) at failure in a beam or plate with a rectangular cross-section is:

$$\left(\frac{P}{P_\ell}\right)^2 + \left(\frac{M}{M_\ell}\right) = 1 \qquad (2.6)$$

where P and M are the applied loads, and P_ℓ and M_ℓ are the limiting values of P and M. The magnitude of P_ℓ and M_ℓ are functions of crack length a, flaw geometry and material properties.

The limit load of P_ℓ is determined from the geometry of the section and the material properties. After the reduction in area due to the flaw is accounted, the limit load can be expressed in terms of a limit stress and the geometric variables. The limit stress is normally the material yield strength when the material behavior is assumed to be elastic-perfectly-plastic. However, for materials which exhibit significant strain hardening, σ_ℓ could be somewhere between yield and ultimate strength, and the appropriate value to use should be determined by tests.

For this analysis, we use a flow stress which is the average of the yield and ultimate strengths, i.e.:

$$\sigma_\ell = (\sigma_y + \sigma_{uts})/2 \qquad (2.7)$$

where σ_ℓ is the flow stress, σ_y the specified minimum yield stress and σ_{uts} the specified minimum ultimate strength.

Once the limit conditions have been calculated, Equation 2.6 and the expressions for applied membrane stress as a function of pressure and applied moment can be used to determine the failure condition.

A limit load evaluation has been made in conjunction with LEFM methods in the present case.

2.1.4 Summary of Fracture Mechanics Background

The failure behavior of structures under monotonic loading can be

classified into three regimes. Of these, linear elastic fracture mechanics has been determined to be most applicable to the current material and service conditions. Bounding studies based on elastic-plastic and plastic limit load analyses have also been performed.

2.2 Fatigue Loading

2.2.1 Analysis Method

The preceding discussion addressed the case of monotonic loading. In the present case, there are a small number of cyclic loads which may occur on the containment structure. This section discusses the way in which these loads can be evaluated in the light of the previous discussion.

Fatigue evaluation, based on fracture mechanics, assumes that initial flaws are present of size a_i and that the lifetime of a component is that required for a crack to grow from the initial size, a_i, to the critical size, a_c. Crack growth rate data may be correlated to the crack tip stress intensity factor range (ΔK) for the given load cycle in the following form:

$$da/dN = f(\Delta K) \qquad (2.8)$$

where da/dN is the crack growth per load cycle. By integrating Equation 2.8 with the appropriate component stress field to calculate K, the number of cycles, N, (residual life) for a crack to grow from a_i to a_c is computed from:

$$N = \int_{a_i}^{a_c} \frac{da}{da/dN} \qquad (2.9)$$

The final flaw size expected at the end of the design life, a_f, can be determined by integrating Equation 2.8, using the appropriate stress distribution to calculate K, and the number of total design cycles N_o from

$$N_o - \int_{a_i}^{a_f} \frac{da}{da/dN} = 0 \qquad (2.10)$$

where Equation 2.10 is a transcendental expression involving a_f and must be solved by an iterative process.

2.2.2 Crack Growth Rate Representation

Many empirical relations to express da/dN behavior have been proposed; the earliest and most well known is the Paris rule (2-11) which takes the form,

$$da/dN = C\Delta K^n \qquad (2.11)$$

where C and n are constants determined from the data, and ΔK is the range of applied stress intensity factor computed from the minimum and maximum stress in the cycle:

$$\Delta K = \Delta K_{max} - \Delta K_{min} \qquad (2.12)$$

The advantage of the Paris relation is that it is simple in form and it fits experimental data well in the middle range of ΔK. A disadvantage of the relationship is that it does not directly account for mean stress effects (R-ratio effect where $R = K_{min}/K_{max}$) which can accelerate fatigue crack propagation. However, these effects are accounted for in the choice of experimental data used in the modeling procedure.

Section 2
REFERENCES

2-1 Wells, A.A., "Notched Bar Tests, Fracture Mechanics and Brittle Strengths of Welded Structures," Houdremont Lecture 1964, British Welding Journal, No. 1 (January 1965).

2-2 Sumpter, J.D.G. and C.E. Turner, "Fracture Analysis in Areas of High Nominal Strain," Proceedings Second International Conference on Pressure Vessel Technology, San Antonio, TX (October 1973).

2-3 Egan, G.R., "The Application of Fracture Toughness Data to the Assessment of Pressure Vesel Integrity," Proceedings Second International Conference on Pressure Vessel Technology, San Antonio, TX (October 1973).

2-4 Burdekin, F.M. and M.G. Dawes, "Practical Use of Linear Elastic and General Yielding Fracture Mechanics With Particular Reference to Pressure Vessels," Conference on Practical Application of Fracture Mechanics to Pressure Vessel Design, Institution of Mechanical Engineers, London, UK (1971).

2-5 British Standards Institution, "Methods for Crack Opening Displacement (COD) Testing." (1972).

2-6 Stuber, A., J.Wellman and S. Rolfe, "Eighth Progress Report on Application of the COD Test Method to the Fracture-Resistant Design of Pressure Vessels," for Subcommittee on Effective Utilization of Yield Strength of the PVRC, (February 1980).

2-7 British Standards Institution, "Guidance on Some Methods for

the Derivation of Acceptance Levels for Defects in Fusion Welded Joints," Published Document PD 6493:1980.

2-8 Egan, G.R., "Compatability of Linear Elastic (K_{Ic}) and General Yielding (COD) Fracture Mechanics," Engineering Fracture Mechanics, Vol. 15, (1973).

2-9 Merkle, J., "Analytical Applications of the J Integral," ASTM STP 536, American Society for Testing and Materials, (1972).

2-10 Hayes, D.J. and Turner, C.E., "An Application of Finite Element Techniques to Post-Yield Analysis of Proposed Standard Three-Point Bend Fracture Test Pieces," International Journal of Fracture, Vol. 10, (1974).

2-11 Paris, P.C., M.P. Gomez and W.D. Anderson, "A Rational Analytic Theory of Fatigue," The Trend in Engineering, Vol. 13. No. 1 (January 1961).

Section 3
ANALYSIS OF STRESSES

The analytical model discussed in Section 2 requires as input the characterization of the stress state present in the containment shell courses. This section discusses both the primary and secondary stresses. The primary stresses are the applied stresses associated with dead load and cyclic service stresses. The secondary stresses, in this case, are the residual stresses due to welding.

3.1 Secondary Stresses

The welds under consideration are double sided butt welds. A literature review was performed to characterize the resulting distribution of residual stresses in this type of weld. The weld has stress components transverse to the weld and longitudinal or parallel to the weld, each with through-thickness distributions. A schematic of these applicable distributions is shown in Figure 3-1. For this analysis the flaw location was assumed to be at the centerline of the plate which is the location for the maximum transverse stress. The flaw location was also assumed to be at the location of maximum longitudinal stress. The transverse distribution through-the-thickness will vary as shown in Figure 3-1.

Figure 3-2 shows single sided butt weld residual stress data transverse through the thickness. This figure is a composite of normalized experimental data based primarily on work done by Nordell and Hall (3-1). In their work, the base plate was ASTM A212 Grade B (precursor to SA516 Grade 70) with double-V butt welds of E7018 material. The applicable thicknesses tested were 1 inch and 1 5/8 inches, requiring 12 and 30 weld passes, respectively. The two thicknesses demonstrated similar through thickness transverse stress distributions. Also shown in Figure 3-2 are residual stresses measured by others (3-2, 3-3).

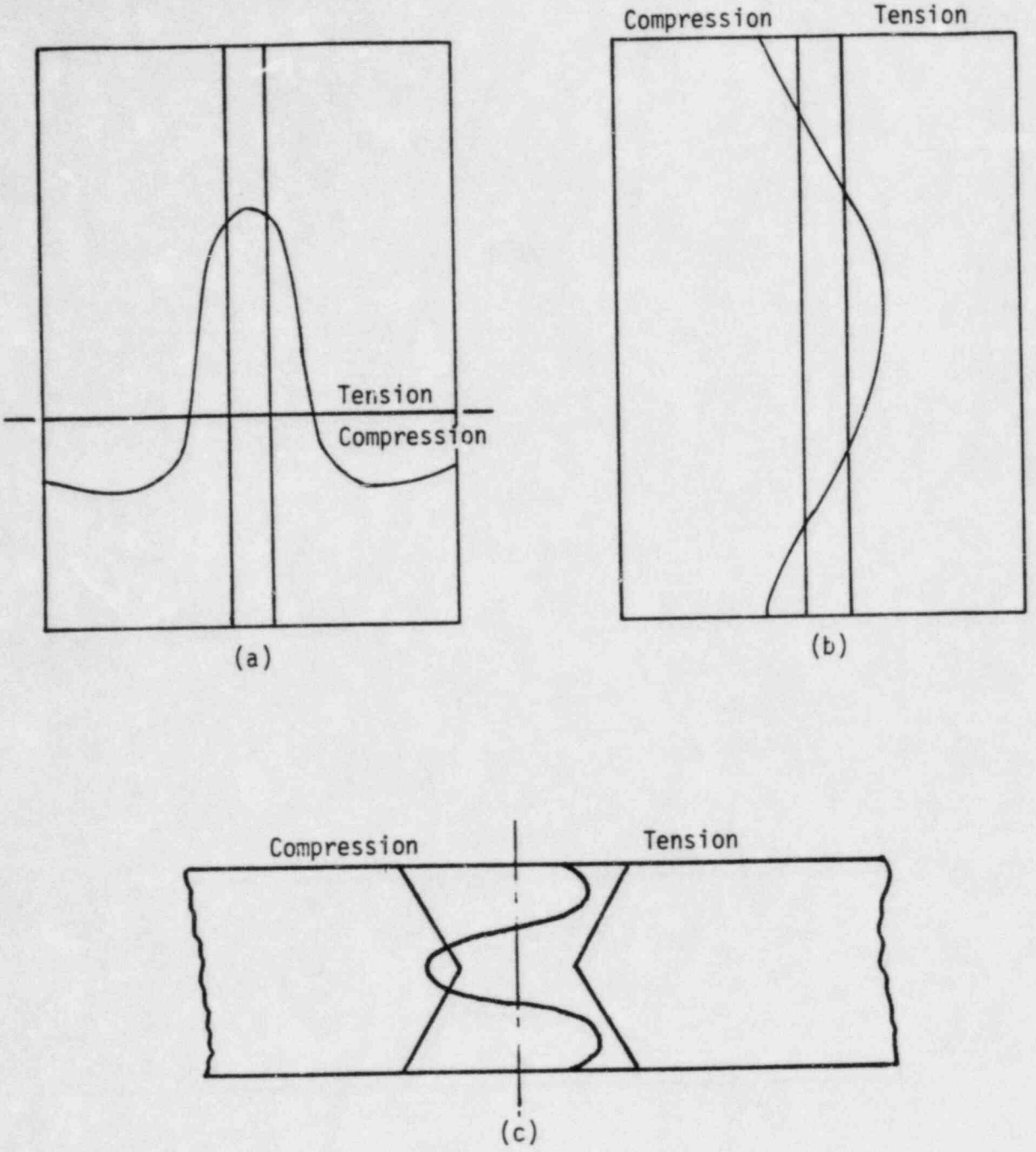

Figure 3-1 Schematic Standard Assumed Residual Stress Distributions in Plates Without Fixed Ends for a Double-Sided Butt Weld: (a) Longitudinal, (b) Transverse, and (c) Transverse Through Thickness.

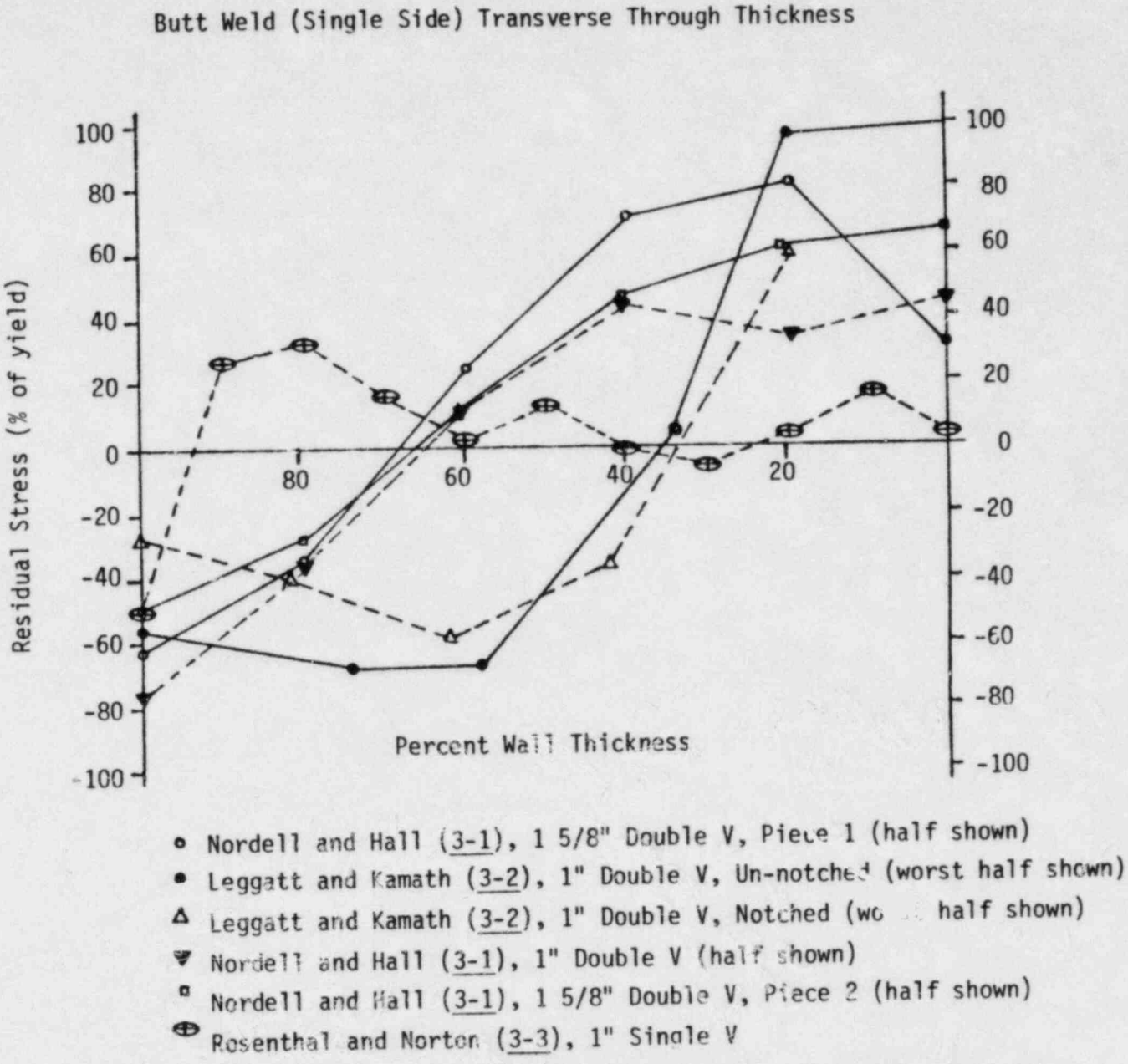

Figure 3-2 Residual Stresses of Single Sided Butt Welds, Transverse Through Thickness

From these data, a simplified through thickness transverse residual stress distribution was developed. This is shown in Figure 3-3. The distribution assumes yield level residual tensile stresses at the surface through 10% of the thickness. The tensile stresses then decrease to compressive residual stresses equal to one half yield at the mid-thickness. This distribution is then reflected about the centerline of the double sided butt weld to achieve a symmetric and complete distribution. Since any residual stress distribution must be self-equilibrating, the choice of values taken here will be conservative. The sum of the tensile portions is larger than the compressive portions and the maximum values have been assumed uniform except in the through thickness direction.

3.2 Primary Stresses

The primary stresses for analysis have been obtained from unit stress calculations for joint 1 (CD-130) for welds 1-1 and 1-2; and from joint 5 (CD-139) for welds 1-4, 1-7, and 1-9. The stresses in welds 1-7 and 1-9 are substantially less than in weld 1-4 (see CD-139 attachment 6). A bounding case has been formulated for welds 1-7 and 1-9 using the stresses in joint 5 (elevation 592'-2"). These stresses are summarized by joint number and Load Combination for each joint and the applicable load combinations. Since the flaws found are oriented parallel to their welds, the stresses in the longitudinal direction apply. A schematic diagram of flaw orientation and applicable stress component is shown in Figure 3-4.

The approach taken was to determine the most highly stressed joint and load combination for the appropriate seam welds. These bounding cases could then be applied to any weld defect, regardless of location, to assure a conservative analysis. In fact, two primary stress distributions were obtained for each weld orientation; one for the fatigue analysis and the other for the fracture analysis.

In order to understand how these stresses were determined, it is necessary to review the tabular stress data as it was provided. Table 3-1 is the

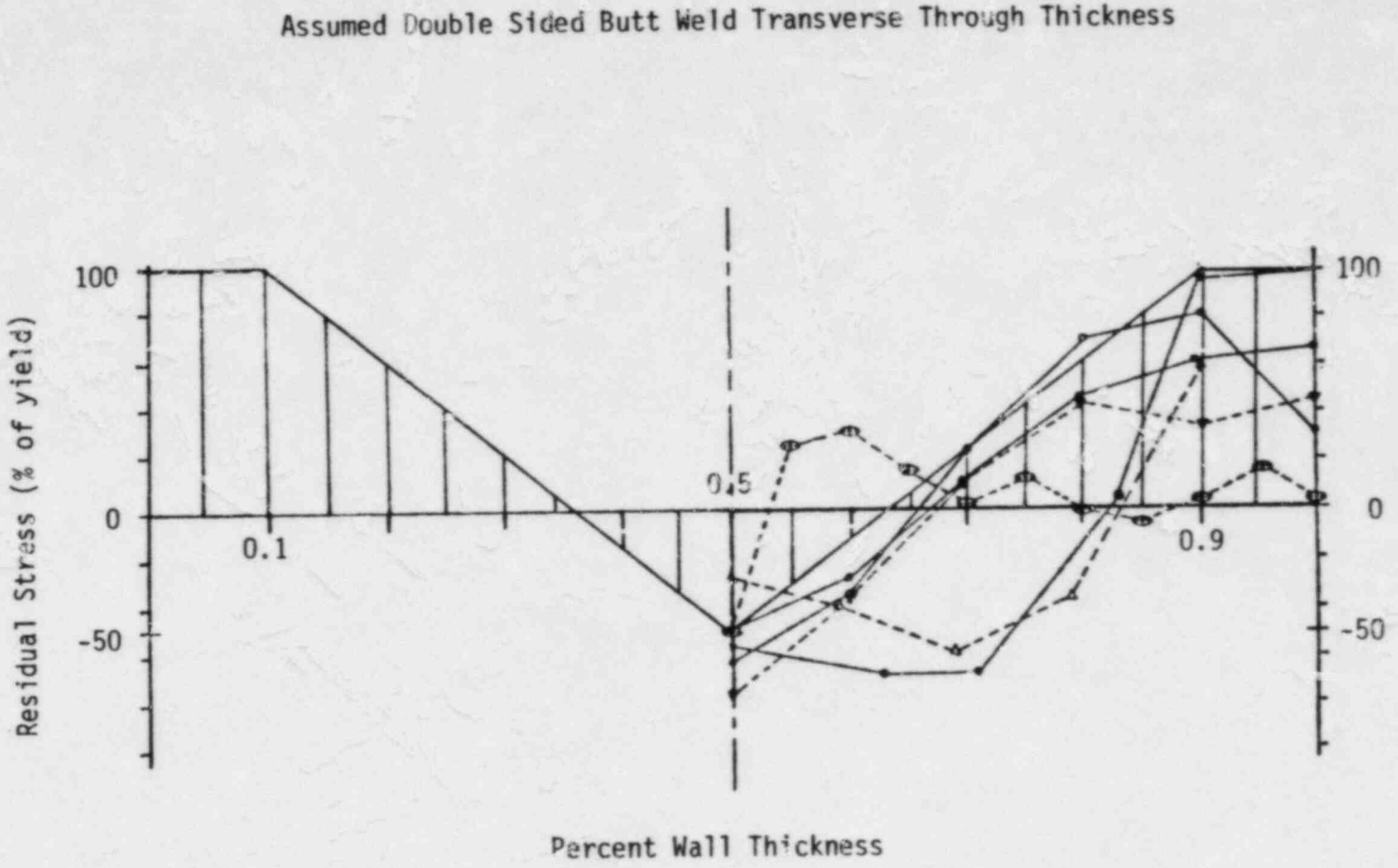

Figure 3-3 Assumed Double Sided Butt Weld Transverse Through Thickness Residual Stress Distribution

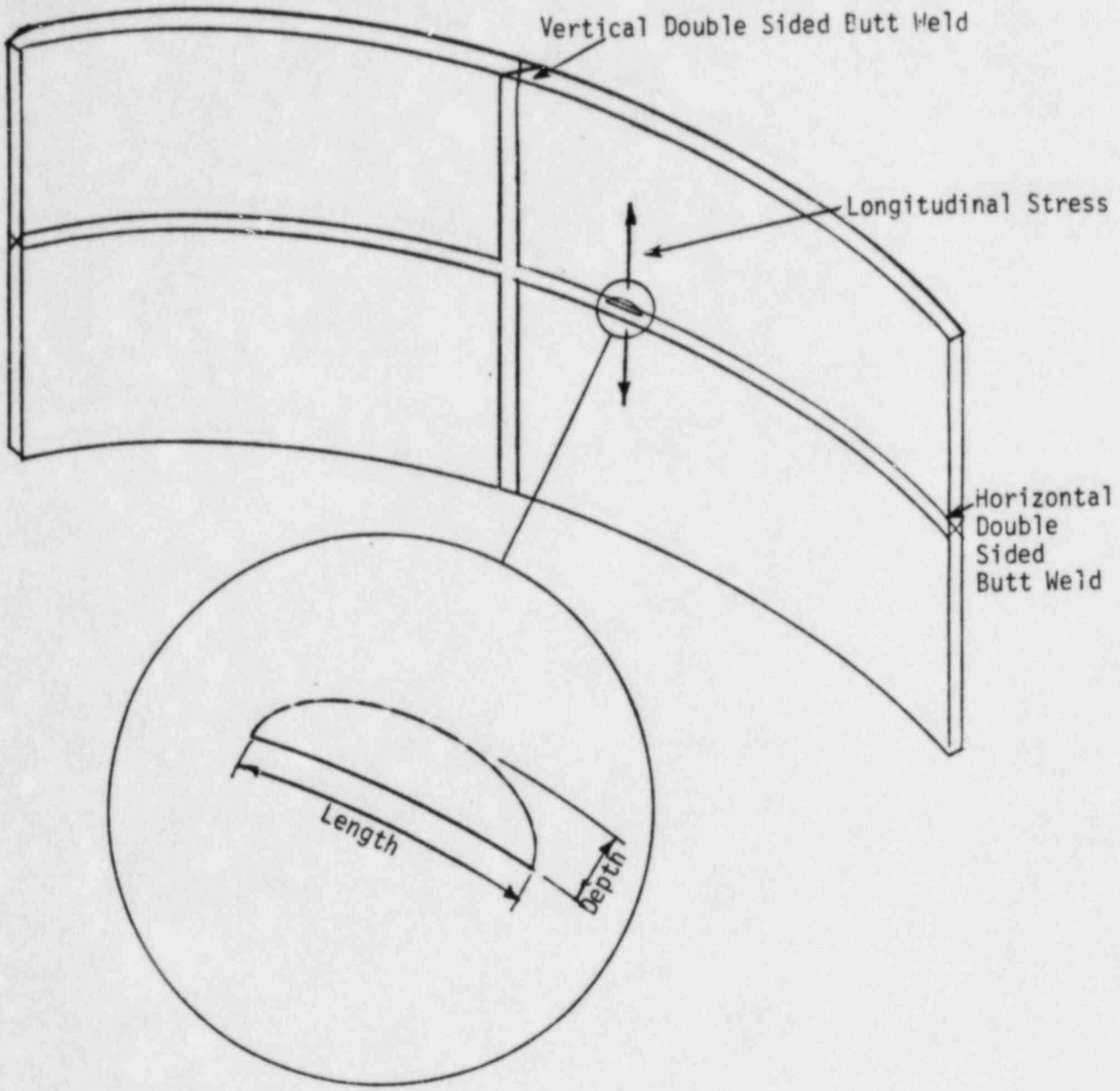

Figure 3-4 Flaw Orientations and Applicable Service Stresses in Vertical and Horizontal Seam Welds

stress summary for Joint No. 5. From this table one can see that the longitudinal and circumferential stresses are broken down into thirteen load components and are then summarized at the bottom of the table into four load combinations. These load combinations represent maximum loading conditions. Some of these load components act at all times, some act cyclically over the life of the plant, and some may act only once. The load components falling into these three categories are summarized in Table 3-2. For a fatigue analysis the cyclic loads are of primary significance and are superimposed with the continuous or steady state loads. For a fracture analysis the most significant loads are those producing the largest stress, which by observation of Table 3-2, are those load combinations that include the single event loads.

Table 3-3 is a summary of the cyclic stresses that govern the fatigue evaluation. There are other cyclic load components. However, the controlling load components in a given load combination are those listed in Table 3-3. Thus, in order to simplify the analysis and provide conservative results, all critical load combinations were evaluated for 16,800 cycles, regardless of which cyclic load components the load combinations include. Table 3-4 shows the appropriate load combination components.

For weld seams 1-1 and 2-1, the stresses taken at joint 1-1 (elevation 575'-1") were used, as shown in Table 3-5. For welds 1-4, 1-7, and 1-9, weld seam 5 stresses were used to bound the applied stress condition. These primary stress fields were combined with the assumed residual stress field for the analysis.

3.3 Combined Stresses

The total stress considered for the evaluation of a defect consists of the sum of the primary and secondary components. Both sets of stresses have been chosen to bound the expected stress state conservatively. For analytical purposes, they have been superimposed with elastic

Table 3-1

Gilbert Associates, Inc. — Reading, Pennsylvania — CALCULATION

SUBJECT: PERRY NUCLEAR POWER PLANT | CISID | PAGE 4 OF PAGES

REV. 0 | MICROFILMED | ORIGINATOR P LUKATE | DATE 2 3 83

JOINT NO. 5 EL 592'-2" - CONT @ 4TH STIFF.

STRESSES IN PSI

LOAD CASE	LONGITUDINAL - σ_ϕ OUTSIDE	LONGITUDINAL - σ_ϕ INSIDE	CIRCUMF. - σ_θ OUTSIDE	CIRCUMF. - σ_θ INSIDE
DEAD LOAD	-1094.	-389.	-335.	-124.
OPERATIONAL BASE EARTHQUAKE	+/- 1836.	+/- 1835.	+/- 854.	+/- 854.
OBE SLOSH	-41.	42.	-14.	11.
OBE - TILTED POOL	-154.	152.	-42.	50.
Σ a + b + c	+1641 / -2031.	+2039 / -1642.	+798 / -910.	+915 / -793.
SAFE SHUTDOWN EARTHQUAKE	+/- 2704.	+/- 2704.	+/- 1260.	+/- 1260.
SSE SLOSH	-82.	84.	-28.	22.
SSE - TILTED POOL	-454.	475.	-126.	162.
Σ a + b + c	+2138 / -3270.	+3263 / -2145.	+1106 / -1414.	+1424 / -1076.
EXTERNAL HYDROSTATIC LOAD DUE TO ANNULUS CONCRETE POUR	68.	-67.	-463.	-503.
15 PSIG STATIC INTERNAL PRESSURE	-454.	7625.	570.	2994.
SRV DISCHARGE - 19 VALVES	+/- 493.	+/- 456.	+/- 221.	+/- 66.
SRV DISCHARGE - ONE VALVE, 1ST POP	+/- 209.	+/- 274.	+/- 129.	+/- 20.
SRV DISCHARGE - 1 VALVE SUBSEQUENT	+/- 361.	+/- 469.	+/- 224.	+/- 33.
MEAN CONDENSATION OSCILLATION	+/- 31.	+/- 27.	+/- 13.	+/- 5.
MEAN CHUGGING	+/- 42.	+/- 43.	+/- 18.	+/- 8.
HYDROSTATIC PRESSURE 18'6"	-81.	80.	-34.	14.
LOCA POOL SWELL	-6813.	8264.	-1136.	3200.
DBA LOCA THERMAL STRESS	-11413.	8461.	-22183.	-16221.
Σ of (1)(2)(4)(7)(11)(12)	-6072 / -10 60.	10192. / 5972.	-1041 / -3007.	2722 / 1974.
Σ of (1)(3)(4)(7)(11)(12)	-5573 / -11299.	11425. / 5469.	733 / -3511.	4251 / 1091.
Σ of (1)(2)(4)(5)(9)(10)(11)	648 / -4127.	9778. / 5108.	775 / -1411.	2270 / 1514.
Σ of 1 2 4 5 8 10 11 13	-10930 / -15408	18252 / 13558	-24057 / -23597	-12884 / -14674

+ Tension
- Compression

Table 3-2

CLASSIFICATION OF LOAD COMPONENTS BY FREQUENCY OF OCCURRENCE

Continuous or Steady State Loads

Dead Load

External Hydrostatic Load Due to Annulus Concrete Pour

Hydrostatic Pressure 18'-6"

Cyclic Loads

OBE

SSE

SRV Discharge - 19 Valves

SRV Discharge - One Valve, 1st Pop

SRV Discharge - One Valve, Subsequent

Mean Condensation Oscillation

Mean Chugging

Single Load Events

LOCA Pool Swell

DBA LOCA Thermal Stress

15 psig Static Internal Pressure

Table 3-3
SUMMARY OF CYCLIC STRESSES

SOURCES	NUMBER OF OCCURRENCES	NUMBER CYCLES PER OCCURRENCE	TOTAL NUMBER OF CYCLES
SRV Actuation	1860	9	16,740
OBE	5	10	50
SSE	1	10	10
TOTAL			16,800

Table 3-4
LOAD COMBINATIONS EVALUATED FOR ANALYSIS

Load Combination Number	Load Components
I	DL + OBE + CONC + SRV_1 + HYDRO + PS
II	DL + SSE + CONC + SRV_1 + HYDRO + PS
III	DL + OBE + CONC + SIP + SRV_{19} + CHUG + HYDRO
IV	DL + OBE + CONC + SIP + SRV_2 + CHUG + HYDRO + LOCATHERM

DL	=	Dead Load
OBE	=	Operating Basis Earthquake
SSE	=	Safe Shutdown Earthquake
CONC	=	External Hydrostatic Load Due to Annulus Concrete Pour
SIP	=	15 psig Static Internal Pressure
SRV_{19}	=	SRV Discharge - 19 Valves
SRV_1	=	SRV Discharge - One Valve, First Pop
SRV_2	=	SRV Discharge - One Valve, Subsequent Pop
CHUG	=	Mean Chugging
HYDRO	=	Hydrostatic Pressure 18'-16"
PS	=	LOCA Pool Swell
LOCATHERM	=	DBA LOCA Thermal Stresses

Table 3-5
BOUNDING SERVICE STRESSES FOR JOINT 1-1

Location	Stress (psi) Inside	Outside
Stress Component		
Thermal	633	-5857
Hydrostatic	421	-818
Design Pressure	2794	836
Dead Load	-492	-659
PSRV	1085/-1847	-2078/3639
CO	146	279
SSE	±731	±2194
OBE	±555	±1664

Load Combination	Stress Range (psi)	
I	1569/-2473	-1891/498
II	1805/-2709	-1361/-32
III	4509/175	-776/1055
IV	5142/808	-6633/-4802

(From CD-130) Gilbert Ref. Letter PY-STR-1555

perfectly-plastic material behavior.

The cyclic (primary or service) stresses are added to the residual stress distribution such that the maximum stress does not exceed the assumed yield stress of the material. The yield stress used for developing this distribution is 78.6 ksi (see Section 5).

Section 3
REFERENCES

3-1 Nordell, W.J. and W.J. Hall, "Two Stage Fracturing in Welded Mild Steel Plates," Welding Research Supplement, March 1965, Pp. 124-S to 134-S.

3-2 Leggatt, R.H. and M.S. Kamath, "Residual Stresses in 25 mm Thick Weld metal COD Specimens in the As-Welded and Locally Compressed States," The Welding Institute, Report 145/1981, June 1981.

3-3 Rosenthal, D. and J.T. Norton, "A Method of Measuring Triaxial Residual Stresses in Plates," Welding Research Supplement, May 1945, Pp. 295-S to 307-S.

Section 4
FATIGUE CRACK GROWTH RATES

In order to estimate the maximum extent of crack growth that could occur at an indication over the design life of the plant, a fatigue evaluation was performed. This evaluation combined the cyclic stresses (Section 3) with the appropriate crack propagation rates (Section 4) to obtain the expected crack growth (Section 7).

The purpose of this section is to assess propagation rates for defect growth by a fatigue mechanism. With the exception of the possible plate defect in weld joint 1-4, the defects are located in weldments, thus requiring an evaluation of carbon steel weld material crack growth data. References have been drawn together to estimate a conservative (that is fastest possible) bound on potential crack growth. Although no data are available for the exact condition in effect, significant studies have been performed to permit bounding values to be estimated.

The following engineering unit conventions are in effect unless otherwise stated:

- ΔK (stress intensity factor range), ksi $\sqrt{\text{in}}$
- T (temperature), °F
- da/dN (crack growth rate), inches/cycle

All weldments evaluated are composed of E7018 weld metal. Data available in the literature were collected for all types of carbon steel weld metal with an emphasis on E7018. A study by Maddox (4-1), resulted in a substantial amount of crack growth data for four different weld metals including E7018. The four types of test specimens from Maddox are

summarized in Table 4-1 and the crack growth data for these specimens are plotted in Figure 4-1. Crack growth data for the E7018 weld material (weld metal C) are shown separately in Figure 4-2. Also shown on Figure 4-1 is the bounding line from similar testing on plain steels performed by Gurney (4-2).

Other data from similar weld metals (4-3) with and without stress relief, fall within the upper bound shown in Figure 4-1 for Gurney (4-2). The literature also states that weld metals for joining steels such as A516 Grade 70 exhibit slower fatigue growth rates than the base metals (4-4).

Residual stresses may increase crack growth rate (da/dN), but if these stresses are included in estimating crack growth rates, the data indicate that the bounding line by Gurney (4-2) will conservatively predict crack growth for E7018 weldments. Figure 4-3 shows Gurney's upper bound which is represented by:

$$da/dN = 2.63 \times 10^{-10} \Delta K^{3.44} \qquad (4.1)$$

The lamination-like defect in weld 1-4 may propagate in either weld material or SA516 Gr. 70 base plate material depending on the exact defect location and orientation relative to the weld. Both cases were analyzed to bound the possible effects. The growth rate used for SA516 Gr. 70 material was derived in previous work for Gilbert Associates (4-5), based on bounding curves developed from work by Bamford (4-6), and ASME Code Section XI (4-7). This work provides a three point curve depending on the relevant cyclic stress range.

$$da/dN = 3.8 \times 10^{-10} \Delta K^{3.76} \qquad \Delta K < 4.9$$

$$da/dN = 4.4 \times 10^{-13} \Delta K^{8.0} \qquad 11 > \Delta K > 4.9$$

$$da/dN = 3.16 \times 10^{-6} \Delta K^{1.4} \qquad \Delta K > 11$$

Table 4-1

TEST SPECIMENS FROM MADDOX*

WELD METAL	AWS/ASTM CLASSIFICATION	YIELD STRESS (ksi)	ULTIMATE STRESS (ksi)	
A	None	74.4	88.0	A MIG deposit using CO_2 gas shielding and 1 mm diameter wire Type A-17 to BS 2901, Part 2, 1960.
B	E7013	68.3	73.9	A manual metal arc deposit of medium strength using a BS 1719 Class E317 rutile coated electrode.
C	E7018.G	67.2	82.9	A manual arc deposit of medium strength using a BS 1719 Class E614 HJ low hydrogen electrode.
D	E9018.G	89.6	105.3	A manual metal arc deposit of high strength made using a BS 1719 Class E614 HJ low hydrogen electrode.

*Ref. (4-1)

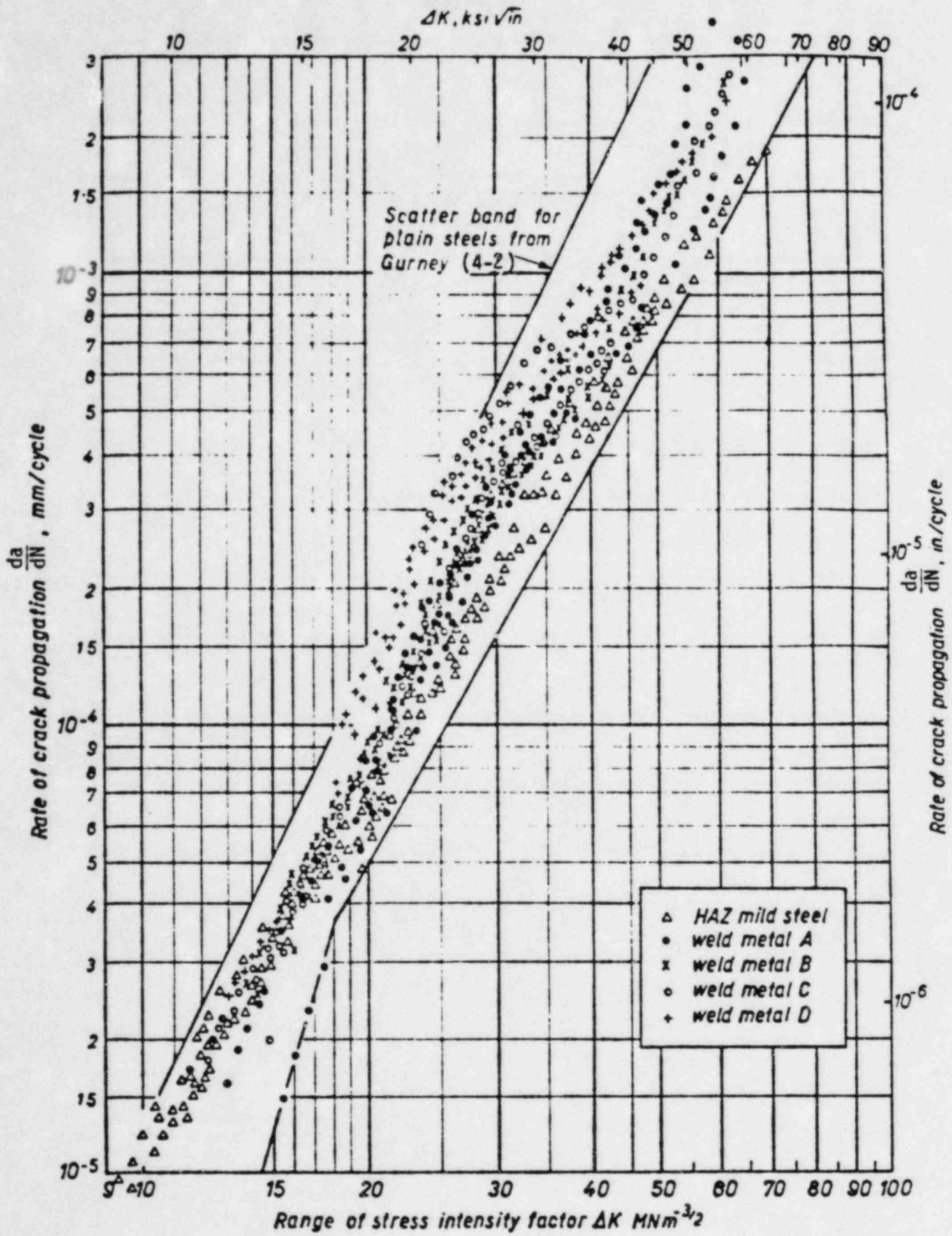

Figure 4-1 Crack Growth data from Maddox (4-1)

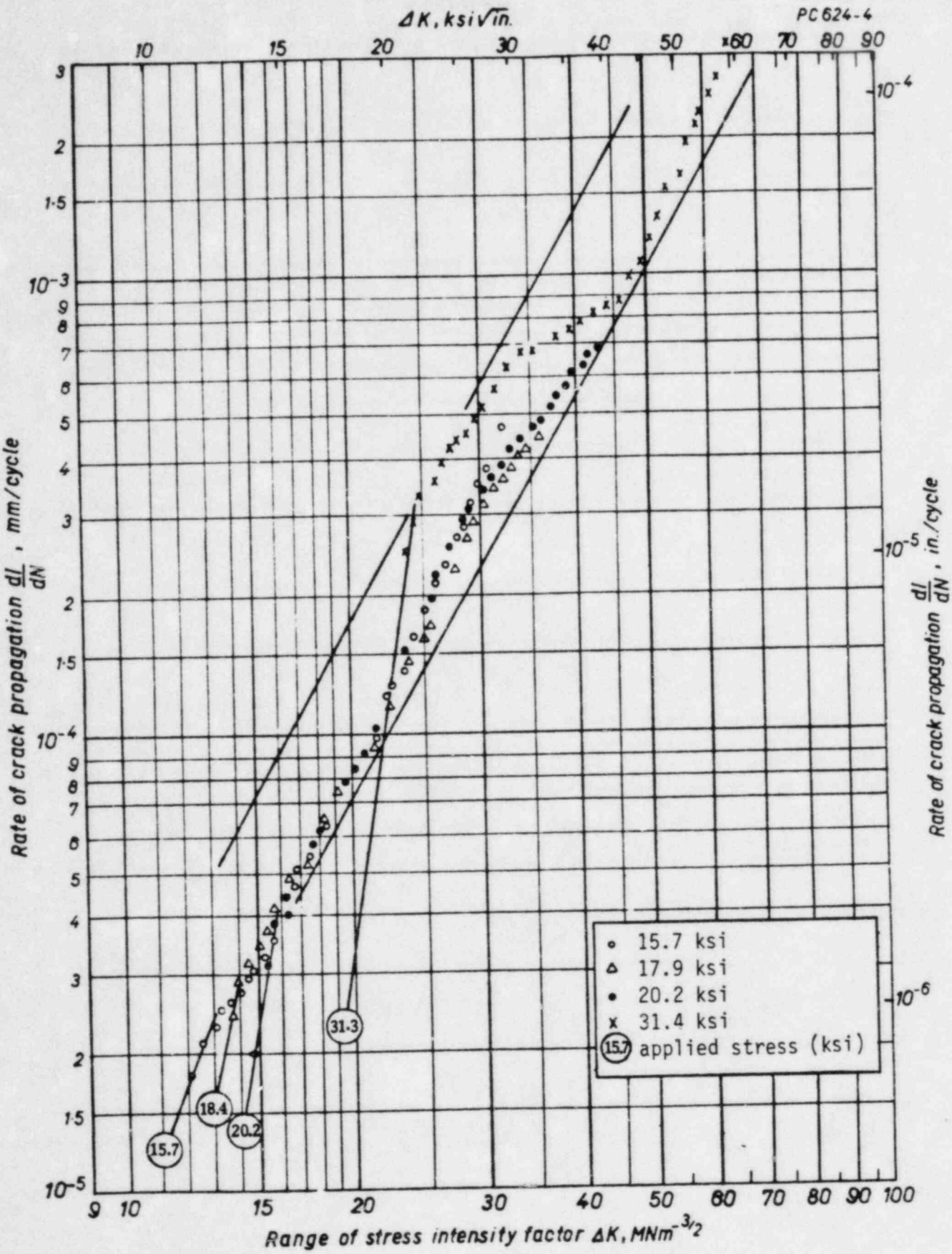

Figure 4-2 Crack growth data for E7018 from Maddox (4-1)

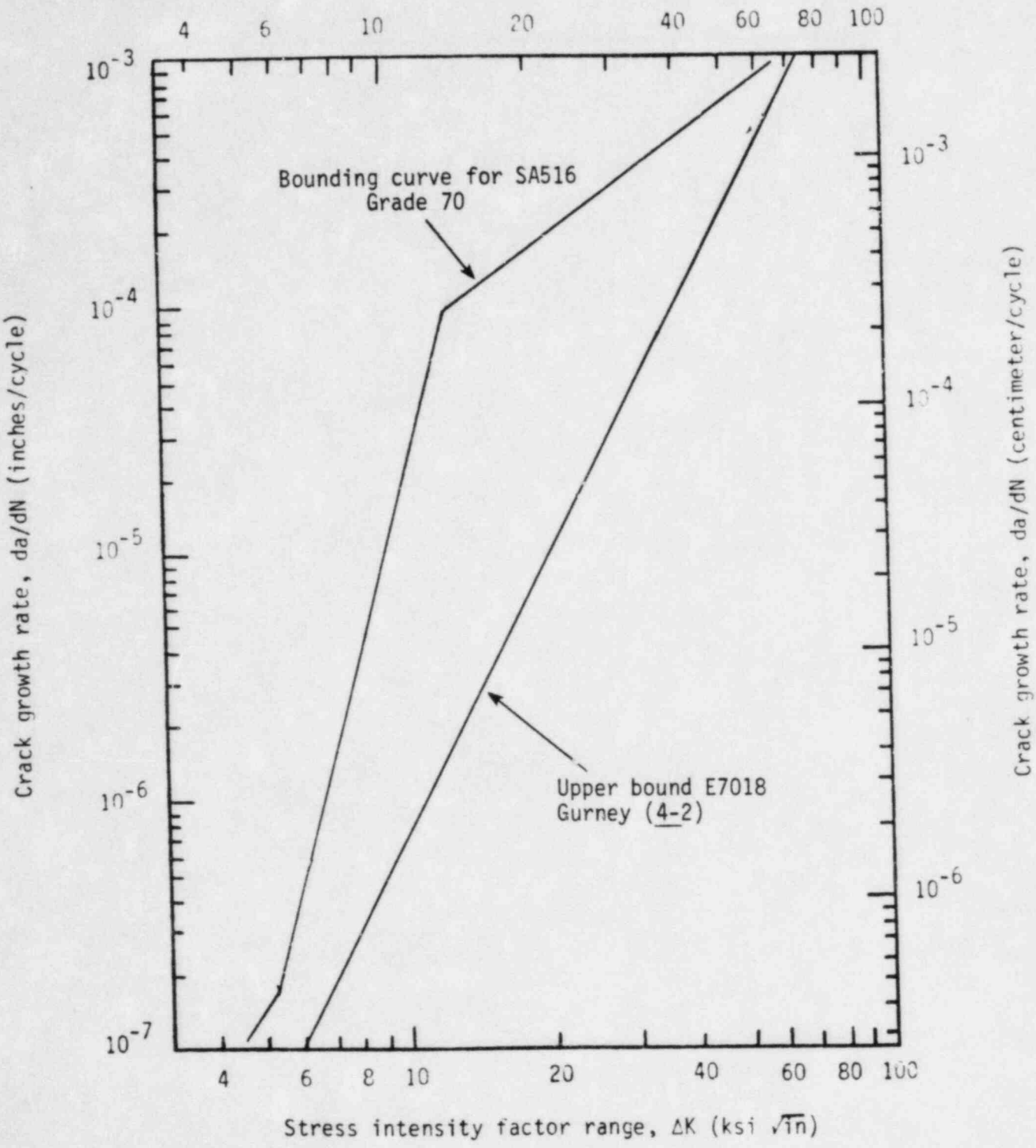

Figure 4-3 Bounding Crack Growth Lines for E7018 weld metal and SA516 Grade 70 base material

These values are shown in Figure 4-3. It should be noted that this curve is very conservative relative to all experimental data reviewed and will provide even more conservative results than the weld metal curve also shown in Figure 4-3.

Section 4
REFERENCES

4-1 Maddox, S.J., "Fatigue Crack Propagation in Weld Metal and Heat Affected Zone Material," The Welding Institute, Report No. E/29/69, Abington, Great Britain, 1969.

4-2 Gurney, T.R. and S.J. Maddox. "A Reanalysis of Fatigue Data for Welded Joints in Steel," The Welding Institute, Welding Research International, Vol. 3, No. 4, 1973.

4-3 Seeley, R.R., L. Katz and J.R.M. Smith, "Fatigue Crack Growth in Low Alloy Steel Submerged Arc Welds," Fatigue Testing of Weldments, Pp. 261-284.

4-4 Gurney, T.R., "An Investigation of the Rate of Propagation of Fatigue Cracks in a range of Steels," The Welding Institute Members' Report No. E18/12/68.

4-5 Egan, G.R., et. al., "The Significance of Sensitized Stainless Steel Material in Drywell Vent and Containment Structures in the Perry Nuclear Power Plant - Fracture and Fatigue Evaluations," AES Report 81-11-88, November, 1981.

4-6 Bamford, W.H., "Application of Corrosion Fatigue Crack Growth Rate Data to Integrity Analysis of Nuclear Reactor Vessels," American Society of Mechanical Engineers, Paper No. 79-PVP-116, 1979.

4-7 American Society of Mechanical Engineers, Boiler and Pressure Vessel Code, Section XI.

Section 5
FRACTURE TOUGHNESS AND STRENGTH

5.1 Introduction

Two additional model inputs to be discussed are the material properties; fracture toughness and strength. As discussed in Section 2, the applied stress intensity is compared to a critical value which is defined as the fracture toughness. Thus, to determine allowable flaw sizes, the fracture toughness must be characterized. Although no direct measurements of fracture toughness were performed in the course of this work, inference about the level of fracture resistance inherent in the material can be made by reference to the Charpy impact values which are available. The background is presented in Section 5.2. The data are discussed in Section 5.3 for the containment welds and base plates (for possible plate delamination of weld 1-4). Section 5.4 analyzes typical crack opening displacement values to be used in the elastic-plastic fracture mechanics evaluation. Section 5.5 addresses the yield and ultimate strength values to be used in the limit load assessment. Certified Material Test Reports (CMTR's) (CD-4, CD-7, and CD-127) were analyzed to determine Charpy (CVN), yield strength and tensile strength data. Controlled document 127 was provided specifically to confirm the CMTR's for E7018 used in Weld Joint 1-1 between seams 21-22 where the largest defects occurred. CD-4 and CD-7 were obtained in previous work for Gilbert and list data for many heats of E7018 used in containment welds. These data have also been included (see Table 5-1) to indicate the variation in material properties.

5.2 Fracture Toughness: Background

To use the analyses described in Section 2.0, it is necessary to have the appropriate value of material fracture toughness in terms of the critical plane strain stress intensity factor (K_{Ic}). Because of the excellent toughness in this material, these data are not normally available for weld metals such as E7018 at temperatures around 70°F. Valid K_{Ic} data for

Table 5-1

SUMMARY OF WELD PROPERTIES BY HEAT
(AS-WELDED)

WELD WIRE QC#	CMTR#	YIELD STRENGTH (KSI)	LIMIT STRESS (KSI)	AVERAGE CVN (FT/LBS)	TEMP. (°F)
77NNI518	456	66.3	72.3	77.3	-30
77NNI540	472	78.1	83.2	69.8	-30
77NNI563	493	63.4	70.3	45.0	-30
78NNI004	552	68.8	75.7	82.6	-20
78NNI013	557	65.8	72.0	95.2	-20
78NNI014	557	68.4	74.3	109.6	-20
78NNI015	557	65.3	69.9	24.0	-20
78NNI016	557	65.5	71.4	85.0	-20
78NNI024	625	65.3	69.9	24.0	-20
*78NNI100	596	78.1	80.7	62.0	-20
78NNI163	630	68.2	73.1	76.0	-20
78NNI164	630	63.8	69.0	115.3	-20
78NNI202	646	66.9	71.5	120.2	-20
78NNI221	653	68.1	73.9	86.8	-40
*78NNI224	655	66.3	72.6	101.0	-20
78NNI255	663	70.2	73.6	118.4	-20
79NNI016	694	84.9	89.8	66.7	-20
79NNI017	694	78.6	83.3	92.7	-20
79NNI018	694	67.2	72.7	114.0	-20
79NNI099	710	64.5	71.3	84.6	-20
79NNI100	710	70.9	76.4	102.4	-20
79NNI131	716	72.7	79.2	80.3	-20
79NNI161	729	65.3	71.5	56.8	-20
79NNI172	737	65.3	71.5	56.8	-20
80NNI017	746	74.8	79.5	81.0	-20
80NNI050	752	70.0	77.0	69.0	-20
*76NNI182	224	68.9	74.9	42.3	-30
*76NNI218	256	68.5	74.3	85.7	-30
*77NNI058	398	70.0	73.8	138.0	-30
*77NNI519		69.0	73.8	113.3	-30
*77NNI589	520	69.7	73.7	109.7	-30

Taken from CD-4 and CD-7

* Included in CD-127

1.5" thick material are generally only available at temperatures such as -100°F. However, it is possible to infer information about the relative toughness of the present material from available CMTR's. There are several correlations that have been proposed to relate Charpy energy to K_{Ic} values. These include two empirical relationships proposed and verified by Barsom and Rolfe (5-1). The relationship for the transition temperature regime is:

$$\frac{K_{Ic}^2}{E} = 2\,(CVN)^{3/2} \qquad (5.1)$$

where

K_{Ic} = Plane strain fracture toughness (psi $\sqrt{In}$)
E = Young's modulus (psi)
CVN = Charpy V-notch energy (ft-lbs)

The corresponding relationship for the upper shelf regime is:

$$\left(\frac{K_{Ic}}{\sigma_y}\right)^2 = \frac{5}{\sigma_y}\left(CVN - \frac{\sigma_y}{20}\right) \qquad (5.2)$$

where

σ_y = Material yield strength (ksi)
K_{Ic} = Plane strain fracture toughness (ksi $\sqrt{In}$)

Barsom and Rolfe found that at 80°F, the upper shelf correlation was appropriate for all material they tested. All their tests were with material of yield strength greater than 100 ksi, although they claim that Equation 5.2 is valid for materials with yield strength less than 100 ksi if dynamic yield strength is used instead of static yield strength.

Another common correlation, due to Sailors and Corten, which was developed for A533B and A517F (5-2), is

$$K_{Ic} = 15.5\ (CVN)^{0.5} \qquad (5.3)$$

where

K_{Ic} = ksi $\sqrt{in}$
CVN = ft-lb

Pisarski (5-3) who reviewed and verified by experiment ten correlations including those listed above, found that good predictions can be obtained for high strength steels (σ_y > 113 ksi). For lower strength steels, the correlations tend to be generally conservative with the degree of conservatism increasing with decreasing yield strength. Thus, either Equation 5.1 or 5.3 should provide conservative estimates of critical fracture toughness. As a check, relations between critical crack opening displacement value and K_{Ic} are also available from Rolfe and Barsom (5-4) and Egan (5-5), and take the form:

$$\frac{\delta_c}{\varepsilon_y} = \left(\frac{K_{Ic}}{\sigma_y}\right)^2 \qquad (5.4)$$

where

δ_c = Critical crack opening displacement (in.)
ε_y = Yield strain (in/in) = σ_y /E
K_{Ic} = Critical fracture toughness (ksi $\sqrt{in}$)
σ_y = Yield Strength (ksi)

A further evaluation of typical crack opening displacement (COD) values is found in Section 5.4.

5.3 Toughness Values for Containment Welds

Specific certified material test reports (CMTR's) were reviewed only for weld 1-1 between vertical joints 21-22 (CD-127). Furthermore, CMTR's for Perry containment stiffener welds fabricated using E7018 were evaluated in earlier work by APTECH (5-6). These weld data are considered

representative of those that would be found elsewhere in the containment.

There is a large scatter of Charpy V-notch (CVN) data as shown in Table 5-1. The range of test values represented there is 24.0 to 138.0 ft-lbs. The values given for CVN in the table are the "average." This is the average the 5 data points listed in the CMTR or 3 data points if 3 data points are given. In order to be conservative, the lowest CVN value was used to determine fracture toughness (K_{Ic}) of the weld material. Thus, the 24 ft-lbs. corresponds to a Barsom-Rolfe toughness value of 82.6 ksi $\sqrt{\text{in.}}$ With the exception of this one heat, all other heats have calculated K_{Ic} values greater than 132.3 ksi $\sqrt{\text{in.}}$

These values represent tough welds, particularly since the CVN tests were performed at a maximum temperature of -20°F, well below the operating temperature. This fracture toughness value of 82.6 ksi $\sqrt{\text{in}}$ will be conservative since:

- The Barsom-Rolfe correlation used to arrive at these values has been shown to be conservative for materials with these strength levels.
- Most calculated K_{Ic} values using this correlation are substantially above this level.
- The test temperature used to evaluate K_{Ic} is -20°F, whereas a higher temperature during operation will result in correspondingly higher toughness.

A lower bound determination of SA516 Gr. 70 toughness expected in the containment structure was performed in previous work for Gilbert Associates (5-7). This value was found to be 73.2 ksi $\sqrt{\text{in.}}$ The derivation of this result involves considerable conservatism.

Other values determined from Table 5-1 to complete the analysis are yield strength and limit stress. The yield stress is used in determination of residual stresses, as they are a function of yield strength level. The higher the yield strength of the material, the higher the residual stresses. Therefore, the upper bound yield strength is used to determine the maximum possible residual stresses present. The limit strength is used in evaluating the limit load capacity of the structure. The limit strength (σ_ℓ) is defined as

$$\sigma_\ell = (\sigma_y + \sigma_{uts})/2 \qquad (5.5)$$

where σ_y is the yield strength and σ_{uts} is the ultimate strength. For conservatism in the limit load analysis, lower bound values for yield and ultimate strength are used in the determination of the limit strength.

For yield stress, a value 78.6 ksi has been used and for limit stress, 66.0 ksi. (See Section 7.2) The conservatism is apparent in that the prescribed yield stress is 12 ksi greater than the limit stress used in the analysis.

5.4 Crack Opening Displacement (COD) Values

Crack opening displacement testing is used as a direct measure of fracture resistance. Literature data are available to provide typical COD values for E7018. These are presented in Appendix A. These data were used in two ways. First, as a check in the derivation of K_{Ic} and second, as direct input to the EPFM analysis.

A check on derivation of the K_{Ic} value used can be provided by Equation 5.4. From the data in Appendix A, the lowest COD value data at 32°F is .023". For this value of COD, and for $\varepsilon_y = 0.2\%$, $\sigma_y = 63.4$ ksi (the lowest strength material given in Table 5-1), the resulting K_{Ic} value is calculated as:

$$\frac{\delta_c}{\epsilon_y} = \left(\frac{K_{Ic}}{\sigma_y}\right)^2$$

$$K_{Ic} = 214.9 \text{ ksi } \sqrt{\text{in}}$$

Thus, the value of 82.6 ksi$\sqrt{\text{in}}$ taken in Section 5.3 corresponding to a CVN value = 24 ft-lbs., is very conservative.

Section 5
REFERENCES

5-1 Barsom, J.M. and S.T. Rolfe, "Correlations Between K_{Ic} and Charpy V-Notch Test Results in the Transition Temperature Range," ASTM STP 466, (1970), Pp. 281-302.

5-2 Sailors, R.H. and H.T. Corten, "Relationship Between Material Fracture Toughness Using Fracture Mechanics and Transition Temperature Tests," ASTM STP 514, (1973), Pp. 164-191.

5-3 Pisarski, H.G., "A Review of Correlations Relating Charpy Energy to K_{Ic}," The Welding Institute Research Bulletin, (December 1978), Pp. 362-367.

5-4 Rolfe, S.T. and J.M. Barsom, Fracture and Fatigue Control in Structures: Applications of Fracture Mechanics, Prentice-Hall (1977).

5-5 Egan, G.R., "Compatibility of Linear Elastic (K_{Ic}) and General Yielding (COD) Fracture Mechanics," Engineering Fracture Mechanics, (1973), Vol. 5, Pp. 167-185.

5-6 Egan, G.R., W.P. McNaughton and J.D. Byron, "A Fracture Mechanics Analysis of Containment Stiffener Flange Welds in the Perry Nuclear Plant," APTECH Report, AES-82-01-92 (April 1982).

5-7 Egan, G.R., et. al., "The Significance of Sensitized Stainless Steel Material in Drywell Vent and Containment Structures in the Perry Nuclear Power Plant - Fracture and Fatigue Evaluations," AES Report No. 81-11-88, November, 1981.

Section 6
CHARACTERIZATION OF FLAWS

The final input required for the fracture mechanics evaluation is flaw size. The applied stress intensity factor calculated by linear elastic fracture mechanics methods and the net section stress of the limit load method will both require an accurate description of flaw dimensions. This will include both depth and length information. Length information is generally easier to obtain as the projection of length onto film is obtained by standard radiographic methods. Depth data have been less easily obtained without resort to volumetric examination by ultrasonic techniques or destructive testing techniques. For structural integrity evaluations an assumption has been generally imposed that confines the flaw depth to one weld pass in multipass welds for certain defect types. This assumption will be conservative for porosity and slag inclusion defect types. However, in many instances it may be overly conservative. Such an assumption confining the expected defect depth to one weld pass will not however guarantee conservatism for "linear" defects like cracks, lack of fusion and lack of penetration. To more fully characterize both types of defects in the weld joints of interest, a radiographic enhancement technique has been used. This is discussed in Section 6.3 below. The enhancement procedure also allows accurate length sizing of defects. When combined with equations of interaction (discussed below), this allows the analyst to determine if two adjacent defects or a series of defects should be most accurately represented as single imperfections or treated as continuous. The details of defect interaction are discussed in Section 6.2. The following section discusses the effect on structural integrity of the rounded defect types, particularly slag inclusions.

6.1 The Effect of Slag Inclusions on Structure Integrity

Work by Harrison (6-1) has indicated that slag inclusions have little effect on the tensile strength of butt welds up to considerable percentages

of cross-sectional area. In support, he shows results of work by Ishii (6-2) and by Kihara (6-3). These results are shown in Figure 6-1. Harrison further points out that by their nature slag inclusions are unlikely to occupy a large proportion of the cross-sectional area of a given weld and the weld metal will usually overmatch the base metal in strength. The conclusion to be drawn from these factors is that the effect of slag inclusions on static tensile strength in materials like E7018 is negligible. Harrison confirms that size-for-size, slag inclusions will be less detrimental than cracks because of their roundness and limitations on their through-thickness size.

A similiar conclusion is reached considering low cycle fatigue. Work by Ishii and Iida (6-4) is shown in Figure 6-2 and indicates that slag inclusions have little effect on load-controlled low-cycle fatigue and up to lives of about 10^4 cycles. The design can thus be based on the static tensile behavior. For the analysis of these inaccessible defects, the structure may be subjected to as many as 18,600 cycles. This is still considered low-cycle fatigue for the purposes of our analysis, and the effect of slag inclusions will be well characterized by the static loading case, particularly in light of the relatively low magnitude of the cyclic stresses (relative to the fully reversed limit level stresses used to generate the S-N curves of Figure 6-2). Additional results given in figures 6-3 though 6-5 indicate the effects on fatigue strength for high cycle fatigue. The number of cycles required to enter a regime characterized by substantial effects on life is shown to be at least an order of magnitude greater than the design life in the present case.

In summary, Harrison (6-1) states that there seems to be sufficient evidence to indicate that under load-controlled conditions, low-cycle fatigue is not a problem which will be influenced by the presence of slag inclusions.

The tensile strength, σ_u, of a defective butt weld will be either

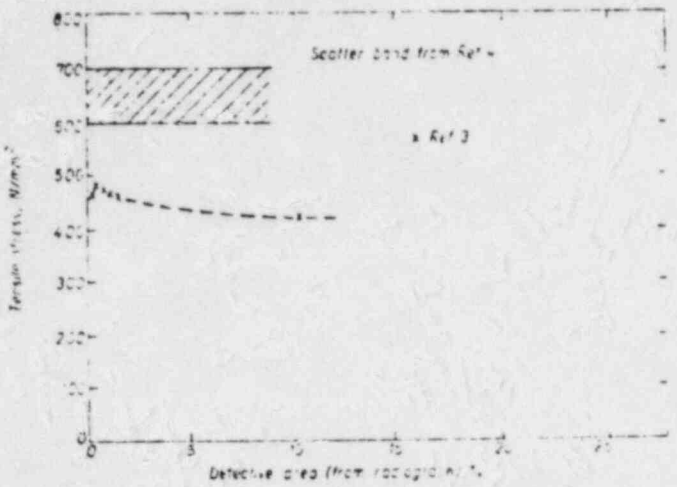

Figure 6-1 Effect of Slag Inclusions on Tensile Strength (taken from 6-1)

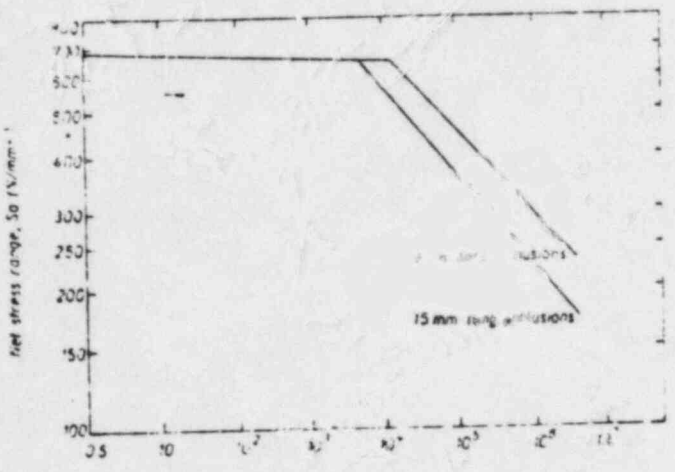

Figure 6-2 Results of Load-Controlled Repeated Stress Fatigue Tests on Butt Welds Containing Slag Inclusions (taken from 6-1)

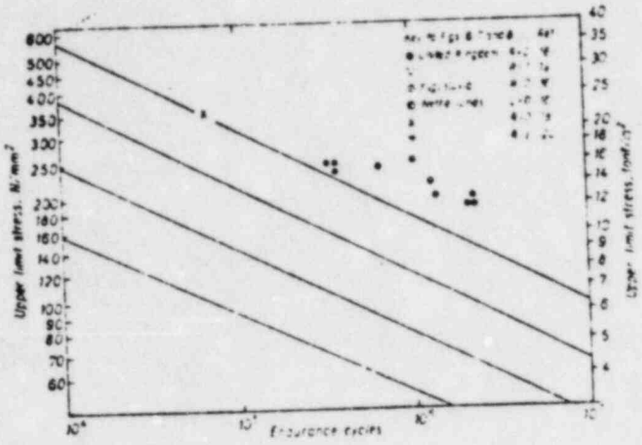

Figure 6-3 Results of Tests on Low-Hydrogen Welds Containing Slag Inclusions up to 5mm Long (taken from 6-1)

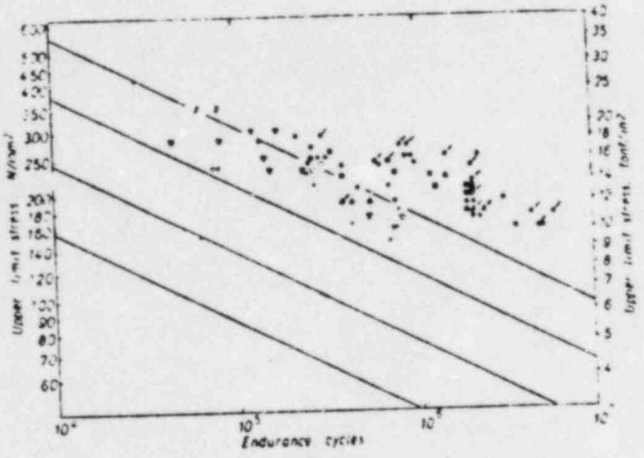

Figure 6-4 Results of Tests on Low-Hydrogen Welds Containing Containing Slag Inclusions up to 25mm Long (taken from 6-1)

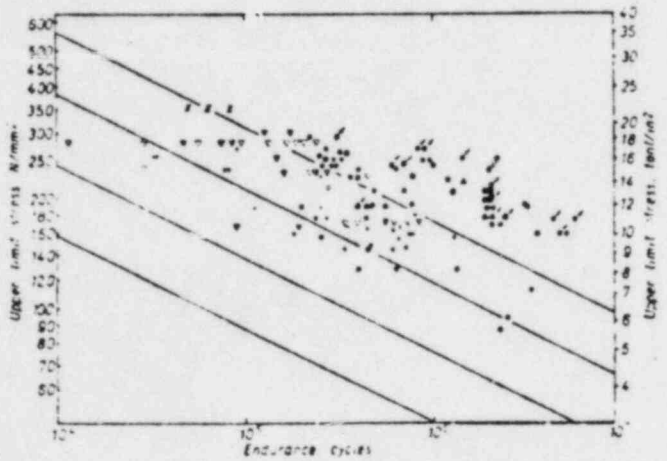

Figure 6-5 Results of Tests on Low-Hydrogen Welds Containing Slag Inclusions up to Continuous Slag Lines (taken from 6-1)

$$\sigma_{u,w} \quad (1 - \Delta A/A)$$

or $\sigma_{u,p}$

whichever is least. Where:

$\sigma_{u,w}$ = the tensile strength of the weld metal

$\sigma_{u,p}$ = the tensile strength of the parent material

$\Delta A/A$ = ratio of the loss of area due to porosity or slag inclusion to the total area

The effect of porosity on structural integrity is similiar to that for slag inclusions. Figure 6-6 shows the effect on tensile strength of a weld as a function of volume of pores. This figure is from work by Harrison (6-5). Figure 6-7 shows the effect on fatigue life for porosity defects for the case of low cycle fatigue. The behavior is similiar to that for slag inclusions. Harrison concludes for porosity (6-5) that, "There seems to be sufficient evidence to indicate that, under load controlled conditions, low cycle fatigue is not a problem which will be influenced by practical porosity levels." Furthermore:

> "In view of the probable necessity to limit porosity to some percentage probably well below 10% because higher levels would obscure other defects, there is no need to give further consideration to the effect of porosity on static ductile strength. This is because weld metals normally overmatch parent material strength and even where this is not the case the percentage reduction in strength due to porosity is equal to the percentage by volume of porosity and at a maximum of 10% this would not in any normal circumstances be significant."

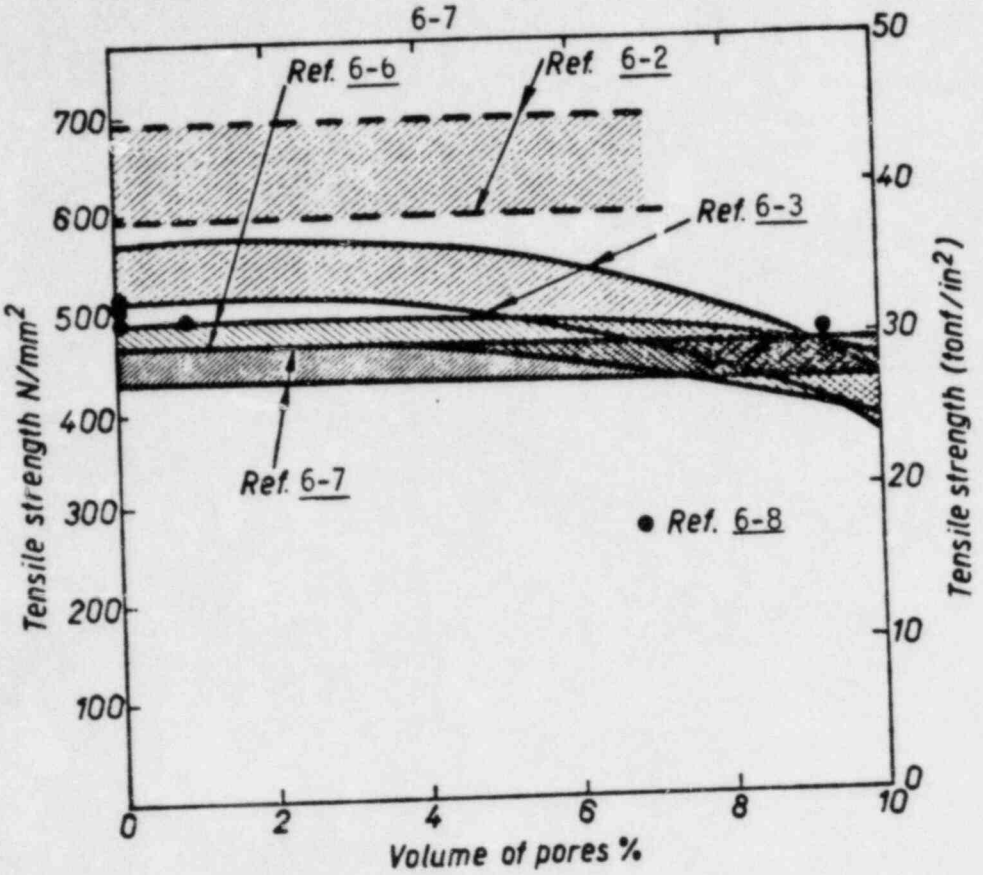

Figure 6-6 Effect of Porosity on the Tensile Strength of Butt Welds (taken from 6-5)

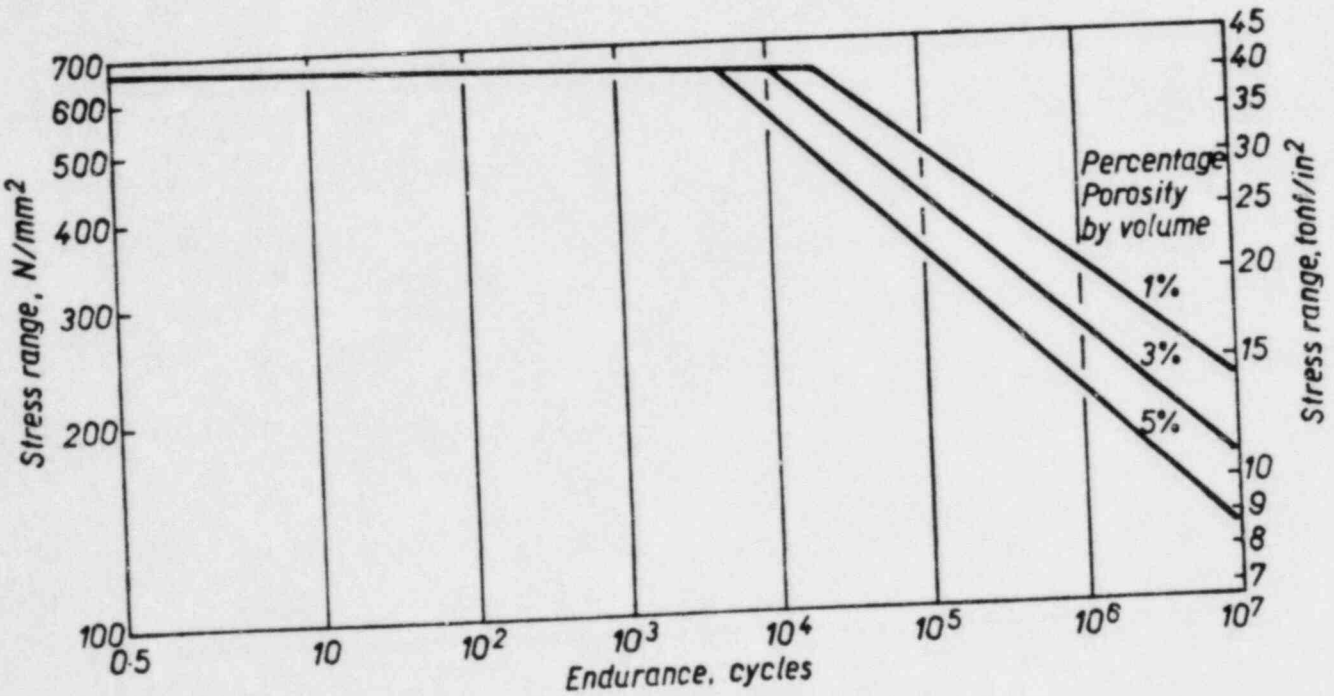

Figure 6-7 Mean S-N Curves for Load Controlled Tests on Porous Welds from Ref. 6- 9 (taken from 6-5)

6.2 Defect Interaction and the Modeling of Defects

In light of the discussion in the previous section it is clear that the rounded defects such as porosity and slag inclusions will have less detrimental effects on structural integrity than linear type defects. However, for the purposes of this analysis we will continue to model the rounded defects as a sharp crack-like defect of the same size. This assumption will lead to a very conservative assessment of the potential for failure as caused by these imperfection types. Thus both linear and rounded defects will be treated as linear imperfections.

Fracture mechanics analyses indicate that the effect of a surface imperfection on structural integrity will be much more severe than that of a buried imperfection. Since we presently have no information about the relative location of the observed imperfections within the weld (in one or two cases some location data are available in the form of ultrasonic inspection records, but generally speaking this additional information is not available). the assumption has been made that the defect is surface-connected. This will give the most conservative result in the calculation of applied stress intensity factors. The model that has been used incorporating these considerations is the surface connected elliptical flaw as shown in Figure 6-8.

The available information which is contained in the radiographs of the welds of interest has been assessed using a computer enhancement system. That procedure is discussed in the following section. However. as a prelude to that discussion some preliminary remarks should be made regarding the interaction of adjacent defects. The British Published Document PD 6493:1980, "Guidance on Some Methods For the Derivation of Acceptance Levels For Defects in Fusion Welded Joints" (6-10) provides perhaps the most complete detailing of interactions between weld defects. A sample of those interactions is shown in Figure 6-9. Of particular interest are the criteria for interaction for the coplanar surface defects and the coplanar embedded defects. As can be seen, if the separation distance, s, was greater than or equal to the mean of the defect lengths

IFI = 305 - ELLIPTICAL SURFACE CRACK

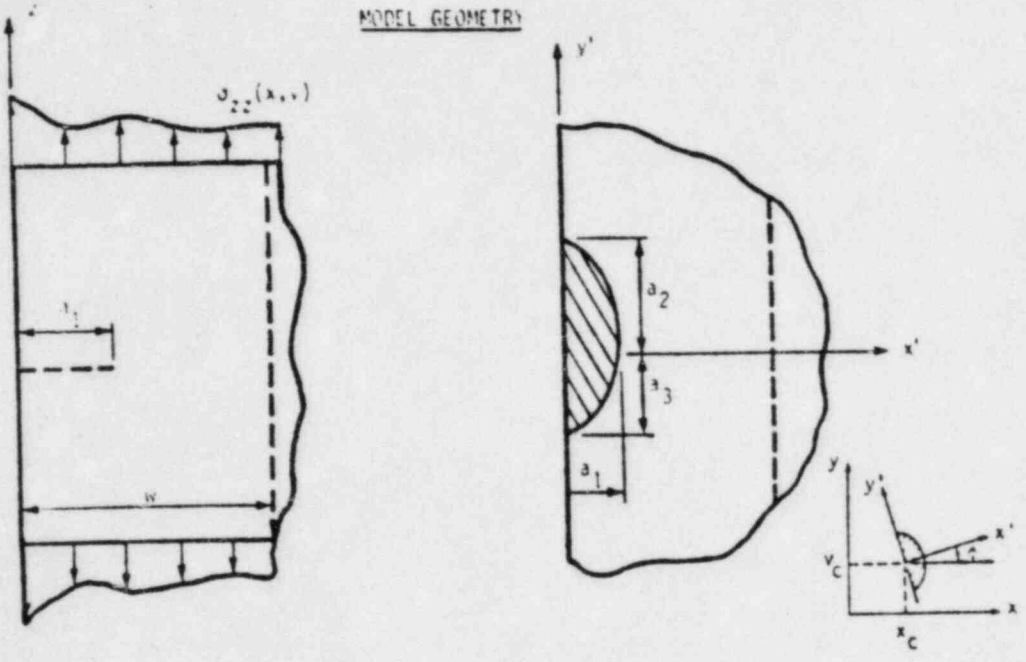

MODEL DESCRIPTION

MODEL FEATURES	PARAMETER	OPTION FEATURED
Model Index Number	IFI	305
Number of Degrees of Freedom	IDOF	3
Crack Front Shape	--	Semi-Elliptical
Crack Opening Mode	--	Mode I
Finite Width Effects	W	No
Variable Thickness Effects	NTH	No

Figure 6-8 Schematic of Surface Elliptical Flaw Model

Schematic defects	Criterion for interaction	Effective dimensions after interaction
1 Coplanar surface defects 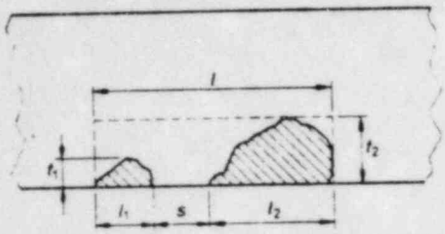	$s \leq \frac{l_1 + l_2}{2}$	$t = t_2$ $l = l_1 + l_2 + s$
2 Coplanar embedded defects 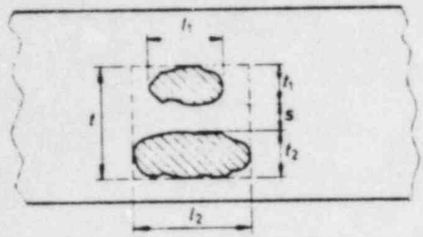	$s \leqslant \frac{t_1 + t_2}{2}$	$t = t_1 + t_2 + s$ $l = l_2$
3 Coplanar embedded defects 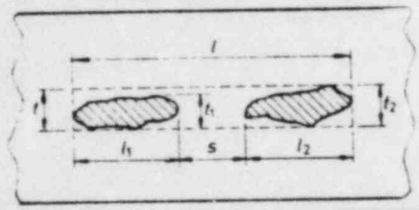	$s \leqslant \frac{l_1 + l_2}{2}$	$t = t_2$ $l = l_1 + l_2 + s$
4 Coplanar surface and embedded defects 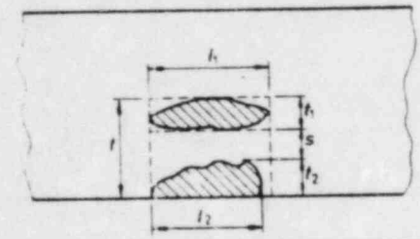	$s \leqslant \frac{t_1}{2} + t_2$	$t = t_1 + t_2 + s$ $l = l_1$
5 Coplanar embedded defects 	$s_1 \leqslant \frac{l_1 + l_2}{2}$ and $s_2 \leqslant \frac{t_1 + t_2}{2}$	$t = t_1 + t_2 + s_2$ $l = l_1 + l_2 + s_1$
6 Coplanar surface and embedded defects 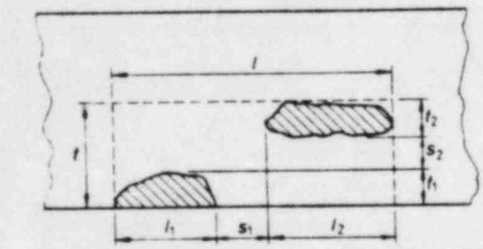	$s_1 \leqslant \frac{l_1 + l_2}{2}$ and $s_2 \leqslant t_1 + \frac{t_2}{2}$	$t = t_1 + t_2 + s_2$ $l = l_1 + l_2 + s_1$

Figure 6-9 Planar Defect Interactions
(taken from 6-10)

then the defects can be treated as separable for the structural integrity analysis. Furthermore, for defects which interact, the maximum defect depth has been taken to be the maximum of the two individual defect depths as indicated in Figure 6-9.

6.3 Digital Enhancement Methods Used in the Present Analysis

Digital enhancement methods have been used in this analysis to provide accurate length and depth values to be used in the fracture mechanics calculations. The image of a radiograph is digitized and then computer manipulated to provide accurate measures of film density. Indications on the radiograph can then be interrogated to determine their extent in the through-thickness direction. By comparing numerical measurements of density of indications with known density changes from image quality indicator wires (penetrameters) or the plate thickness, the depth of indications can be determined. In this case, the density at the defect locations has been compared with the general density of the surrounding weld area to determine the through thickness extent of the defects in terms of a percentage of the weld thickness. A further use of the technique, particularly important in this case, was the use of digital information to determine the extent of weld defects. This was performed by determining the "ends" of any given defect, that is the point at which the density was found to be indistinguishable from that of the weld remote from the defect. Once this location was found then the interaction criteria given in the previous section could be applied to determine the defect length to be used in the fracture mechanics analysis.

The digital enhancement techniques used have been applied to several nuclear applications including both the enhancement of radiographic records and the real time signal enhancement of inspections by remote video camera. Appendix B provides futher information about the previous uses of these techniques and includes a recent paper presented at the International Conference on Fracture Toughness Testing - Methods Interpretation and Application in London, June 9-10, 1982 (6-11), which gives further

background information about the methods used to establish the depth of indications in radiographs.

6.4 Results of the Flaw Characterization

A total of 21 radiographs from weld 1-1, an 43 radiographs from weld 2-1, as well as film for weld 1-4 (79-80) 11-12, were examined using the enhancement techniques discussed above. The results are given in Appendix C, which lists all the welds examined and the maximum defect length and depth found on that radiograph. In many cases, the maximum depth and length were on separate flaws. For example the maximum depth defect was usually a rounded indication, but the longest defect was linear. It should be noted that the resulting bounding or worst case flaws will be much more accurately sized than simply assuming a depth equal to a full weld pass. Furthermore, the linear indications tended to be shallow, although in some cases, relatively long.

In most of the radiographs, the defects were singular or, by analysis using the interaction equations not separable. However, several of the longer defects were separable using the information provided by the digital techniques.

The enhancement work allowed the following worst case defect types, lengths and depths to be entered into the fracture mechanics analysis:

Weld Location	Maximum Length	Depth	Weld ID
Weld 1-1, 2-1			
Inaccessible Defects	4.0"	12.0%	1-1(21-22), 5-6
	1.125"	14.3%	2-1(35-19), 14-15 R1 (slag defect)

Additional Inaccessible Welds			
Weld 1-4,	2.75"	10.0%	Estimate of worst condition from CD-139, attachments 3-5
Welds 1-7, 1-9	1.75"	10.0%	Estimate of worst condition from CD-139, attachments 3-5

Section 6
REFERENCES

6-1 Harrison, J.D., "Basis for a Proposed Acceptance Standard for Weld Defects. Part 2: Slag Inclusions," The Welding Institute, 1972, Abington, Cambridge.

6-2 Ishii, Y., H. Kihara and Y. Tada, "On the Relation Between the Non-Destructive Testing Information of Steel Welds and Their Mechanical Strength." Journal of Non-Destructive Testing (Japan), Vol. 16, No. 8, 1967, Pp. 319-345. IIW Document XIII-466-67.

6-3 Kihara, H., Y. Tada, M. Watanabe, and Y. Ishii, "Non-Destructive Testing of Welds and Their Strength," 60th Anniversary Series. The Society of Naval Architects of Japan, Vol. 7.

6-4 Ishii, Y. and K. Iida, "Low and Intermediate Cycle Fatigue Strength of Butt Welds Containing Defects," Journal of the Society of Non-Destructive Testing (Japan), Vol. 18, No. 10, 1969, IIW Document XII-560-69.

6-5 Harrison, J.D., "The Basis for a Proposed Acceptance Standard for Weld Defects. Part 1: Porosity," The Welding Institute Report 26/3/71, March 1971, Abington, Cambridge.

6-6 Norrish, J. and D.C. Moore, "Porosity in Arc Welds and its Effect on Mechanical Properties," Second Conference on the Significance of Defects in Welds, London, May 1968 (Published by the Welding Institute).

6-7 Green, W.L., M.F. Harmad, and R.B. McCauley, "The Effects of Porosity on Mild Steel Welds," Weld J. Res. Supp. Vol. 23,

No. 5, Pp. 206s-209s.

6-8 Masi, O. and A. Erra, "L'Esame Radiografico delle Saldatura, Una Completa Valutazione dei Diffeti in Termine di Resistenza Statica ed a Fatica," La Metalurgica Italiana, Vol. 45, No. 8, 1953, P. 273-283.

6-9 Ishi, Y. and K. Iida, "Low and Intermediate Cycle Fatigue Strength of Butt Welds Containing Defects," Journal of the Society of Non-Destructive Testing (Japan), Vol. 18, No. 10, 1969. IIW Document XIII-560-69.

6-10 British Standards Institution, Guidance on Some Methods for the Derivation of Acceptance Levels for Defects in Fusion Welded Joints," PD6493:1980, British Standard Institution.

6-11 Egan, G.R., M.F. Elgart and A.A. Smith, "Improved Radiographic Flaw Sizing by Digital Image Processing," International Conference on Fracture Toughness Testing - Methods, Interpretation and Application, June 9-10, 1982.

Section 7
RESULTS OF THE ANALYSIS

The following sections present the results of the analysis which were performed using the methodologies discussed in Section 2.0 and the inputs of Sections 3.0-6.0. The results of the linear elastic fracture mechanics analysis are discussed in Section 7.1, followed by the results of the elastic-plastic and limit load analysis in Sections 7.2 and 7.3 respectively.

7.1 Results of the Linear Elastic Fracture Mechanics (LEFM) Analysis

The LEFM analysis was performed using the BIGIF (Boundary Integral Generated Influence Function) computer program. This program performs the numerical integration of equation 2.10. The program can be used to evaluate the effect of both cyclic and steady state loading on a structure.

7.1.1 Indications in Seams 1-1 and 2-1

Table 7.1 summarizes the input conditions and results for the four bounding cases which were established. For seams 1-1 and 2-1, the maximum length defect could be modeled as 4.0" long and 12% of the weld thickness in depth (see Section 6.4 for details). The worst cyclic stress condition was found (see Section 3.3) to be load combination III (CD-130). These conditions and the bounding fatigue growth rate developed in Section 4.0 were combined in case number 1, which is BIGIF run 1H1. The results are shown in Table 7-1. These indicated that very small growth over the full design life of the plant for these conditions can be expected. The possibility for fracture, given a maximum one time stress loading of this final flaw size was then assessed. The results are listed in Table 7-1 under case 1, run 1H2. The appropriate bounding stress case was load combination IV (CD-130). The results indicate an applied stress intensity factor (K_a) for this bounding case to be 60.0 ksi $\sqrt{in}$. This compares to the critical value 82.6 ksi $\sqrt{in}$ (see Section 5.3). This in turn implies that this size defect will not propagate by a fracture mechanism.

Table 7-1

SUMMARY OF RESULTS

Case	Run No.	Weld Data: Orientation	Weld Data: Seam No.	Joint	Stresses: Load Combination	Bounding Flaw: Length	Bounding Flaw: Depth	Evaluation For[1]	K_a[2] ksi$\sqrt{in}$	K_{IC}[7]/K_a
1	1H1	Horizontal	1-1, 2-1	1	III-ϕ^3	4.0	12%(.180)	Fatigue	60.0	1.37
	1H2	Horizontal	1-1, 2-1	1	IV- ϕ^3	4.0	12%(.180)	Fracture	60.0	1.37
	1H5	Horizontal	1-1, 2-1	1	III-ϕ^3	1.1	14%(.214)	Fatigue	57.5	1.44
	1H6	Horizontal	1-1, 2-1	1	IV- ϕ^3	1.1	14%(.214)	Fracture	57.4	1.44
2[5]	6H1	Horizontal	1-4	5	III-$\phi^{4,9}$	2.75	10%(.150)	Fatigue	54.6[8]	1.34[5]
	6H2	Horizontal	1-4	5	IV- $\phi^{4,9}$	2.75	10%(.150)	Fracture	54.6[8]	1.34[5]
3[6]	6H3	Horizontal	1-4	5	III-$\phi^{4,9}$	2.75	10%(.150)	Fatigue	54.6[8]	1.51
	6H4	Horizontal	1-4	5	IV- $\phi^{4,9}$	2.75	10%(.150)	Fracture	54.6[8]	1.51
4	8H1	Horizontal	1-7, 1-9	5	III-ϕ^4	1.75	10%(.150)	Fatigue	53.4[8]	1.54
	8H2	Horizontal	1-7, 1-9	5	IV- ϕ^4	1.75	10%(.150)	Fracture	53.4[8]	1.54

NOTES:

1. Fracture and fatigue susceptibility checked for worst load combination
2. Maximum at end of design life
3. Taken from CD-130
4. Taken from CD-139
5. Check using base plate growth rates and toughness
6. Check using weld metal growth rate and toughness properties
7. K_{Ic} taken to be 82.6 ksi$\sqrt{in}$ for weld metal, 73.2 ksi$\sqrt{in}$ for base metal
8. Governing case is load combination III
9. Note true applicable stresses will be in "z" direction and thus substantially lower than longitudinal stresses used as bound

A deeper defect was found during the enhancement work. This led to the development of additional computer runs 1H5 and 1H6 using a bounding defect 1.125" long and .214" deep. The resulting value for K_a was less than that for the longer flaw (57.5 ksi $\sqrt{in}$ versus 60.0 ksi $\sqrt{in}$).

7.1.2 Weld 1-4

The plate imperfection of weld 1-4 was modeled using stresses from weld joint 5 (CD-139). Since the location of the imperfection could be affected by either weldment or base plate properties, both possibilites were run. Case 2, runs 6H1 and 6H2, use base plate properties. It should be noted that the actual orientation of the defect is such that stresses to affect it would be the through-thickness stresses which are very small (CD-139). For purposes of this bounding analysis the flaw has been modeled as if oriented normal to the maximum stresses in the longitudinal defect. The results will thus be very conservative when obtained. As with the imperfections in seams 1-1 and 2-1, the combination of stresses and flaw size modeled predicts structural failure will not occur for either set of material properties.

7.1.3 Welds 1-7 and 1-9

It was noted that weld 1-7 is at worst a 9/16" long slag line. In weld 1-9, an excavation for repair was made and that area is not covered by RT to assure repair was completed. Attachment 3 in CD-139 reasons that a bounding case of a flaw 1 3/4" long will bound both 1-7 and 1-9 defects. Case 4 runs 8H1 and 8H2 have been established to evaluate this bounding flaw taken to have a depth equal to .150". The stresses of joint 5 have been used in this evaluation although the true stresses in the upper parts of the containment near joints 1-7 and 1-9 are substantially lower (compare CD-139 attachments 2 and 6). Even with the conservative bounds, this model predicts structural failure will not occur.

7.2 Limit Load Analysis

As discussed in Section 2.0, limit load provides a bounding method of

analysis for structural failure. It is based on two theorems. The first gives rise to lower bound solutions and states that a structure will not fail if the applied forces can be balanced by a redistribution of stress such that the induced stresses do not exceed the yield or flow stress. The second theorem, which is an upper bound theorem, states that the structure will collapse when the rate of external work done by the applied forces exceeds the rate of internal plastic work for any collapse mechanism. As the first theorem provides lower bound results, it will be used in this analysis.

Many solutions have been developed to calculate the critical stress for various geometries and loading conditions using the lower bound theorem. Several of these are reported in (7-1). For a center-cracked plate under uniform tension (Figure 7-1a):

$$\sigma_c = \sigma_\ell(1-2a/t) \tag{7.1}$$

and for a single edge-cracked plate in tension (Figure 7.1b):

$$\sigma_c = \sigma_\ell(1-a/t)\left[1+\ln\left(\frac{1-a/2t}{1-a/t}\right)\right] \quad \text{for } a/t \leq 0.884 \tag{7.2a}$$

and

$$\sigma_c = 2.571\sigma_\ell\,(1-a/t) \quad \text{for } a/t \geq 0.884 \tag{7.2b}$$

These solutions are for infinitely long flaws, which provide overly conservative solutions. The effect of flaw aspect ratio may be considered by replacing a with:

$$\frac{a\left(1-(1+\ell^2/2t^2)^{-\frac{1}{2}}\right)}{1-a(1+\ell^2/2t^2)^{-\frac{1}{2}}/t} \tag{7.3}$$

For the present case, σ_ℓ has been taken to be:

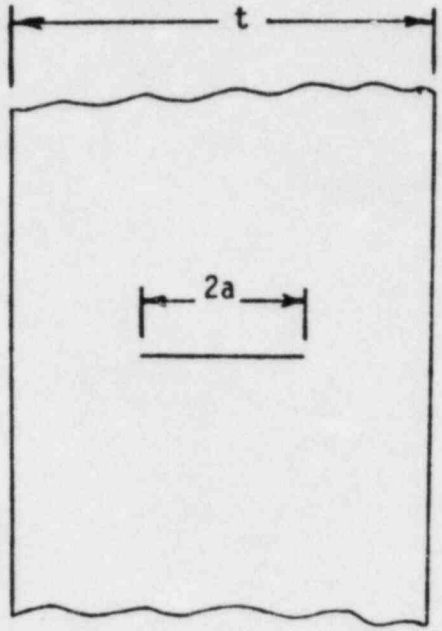

a. Center-cracked Plate

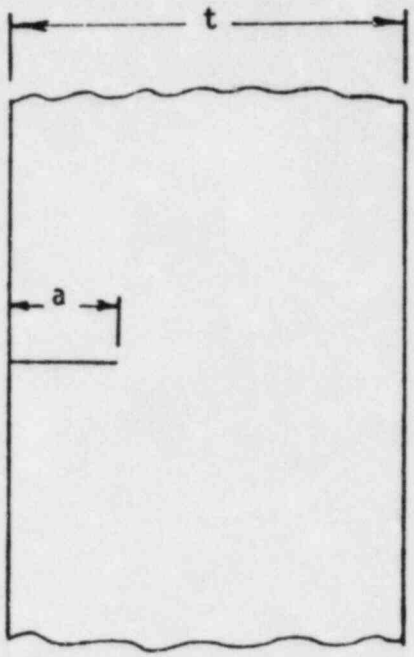

b. Single Edge-cracked Plate

Figure 7-1 Flaw Geometries for Limit Load Analysis

$$\sigma_{\ell} = 1/2(\sigma_y + \sigma_u) \qquad (7.4)$$

Where σ_y and σ_u are the minimum values of yield strength and tensile strength. The minimum limit stress in E7018 can be taken to be 66 ksi which corresponds to the specified minimum tensile and yield strengths of 72 ksi and 60 ksi respectively (taken from AWS A5.1-78 "Specification for Carbon Steel Covered Arc Welding Electrodes" (7-2).

Simplification to the governing equations occurs in this case because any bending stresses applied to the structure will appear as a uniform stress across the section. Further, the size of the detail is sufficiently small so that a crack will not affect the integrity of the structure by net loss of sectional area. Limit load will thus indicate failure when the applied stress in the net ligament is equivalent to the maximum stress which the section will support, or the limit stress. The critical area loss to cause limit load failure was determined from the maximum applied tensile stress. The maximum design tensile stress is found to be in Joint 3, load combination IV, longitudinal stress component σ_ϕ, inside surface and is equal to 33,136 psi (CD-139).

This worst case stress will only result with a section ligament loss of 49.8%. Since the maximum depth defect is 14.3% the ratio of worst defect depth to critical depth is 3.5. Thus, there is a large margin against failure by a limit load mechanism.

7.3 Elastic-Plastic Fracture Mechanics (EPFM) Results

To assure that the linear elastic fracture mechanics analysis was conservative, an EPFM analysis was completed utilizing the concepts outlined in Section 2.1.2. The basis for this analysis is the "Draft British Standard of the Rules for the Derivation of Acceptance Levels for Defects in Fusion Welded Joints" (7-3). Since a rigorous elastic-plastic analysis is very complex compared to LEFM, the Draft Standard has

simplified the procedure by using a semi-empirical design curve set in its current form by Burdekin and Dawes (7-4). Experimental work was performed by Burdekin and Stone (7-5). For a defect in a uniform stress field, the relationships between COD and applied strain are:

$$\phi = (e/e_y)^2, \text{ for } 0 < e/e_y \leq 0.5,$$
$$\phi = e/e_y - 0.25, \text{ for } 0.5 < e/e_y < 2 \qquad (7.5)$$

where ϕ is the non-dimensional COD, i.e.,

$$\phi = \frac{\delta}{2\pi e_y \bar{a}} \qquad (7.6)$$

The COD design curve, shown in Figure 7-2, relates the non-dimensional COD, ϕ, to the ratio of applied strain to yield strain. The applied strain is taken as the local strain which would exist in the vicinity of the crack if the crack itself were not present. It has been shown (7-6) that this design curve is conservative, and thus the allowable flaw size, a, will be a smaller than the critical flaw size, a_{crit}.

The design curve is based on a through-thickness defect (a = through-thickness crack half-length). Although not rigorously justified, it has been suggested that the effect of crack shape is the same for contained yielding problems as for linear elastic problems (7-7). Thus, a pseudo-elastic-plastic solution to part-through cracks can be developed.

For a through flaw with the geometry shown in Figure 7-3a, the LEFM expression is:

$$K_I = \sigma\sqrt{\pi a} \qquad (7.7)$$

For a surface crack with the geometry shown in Figure 7-3b, the LEFM

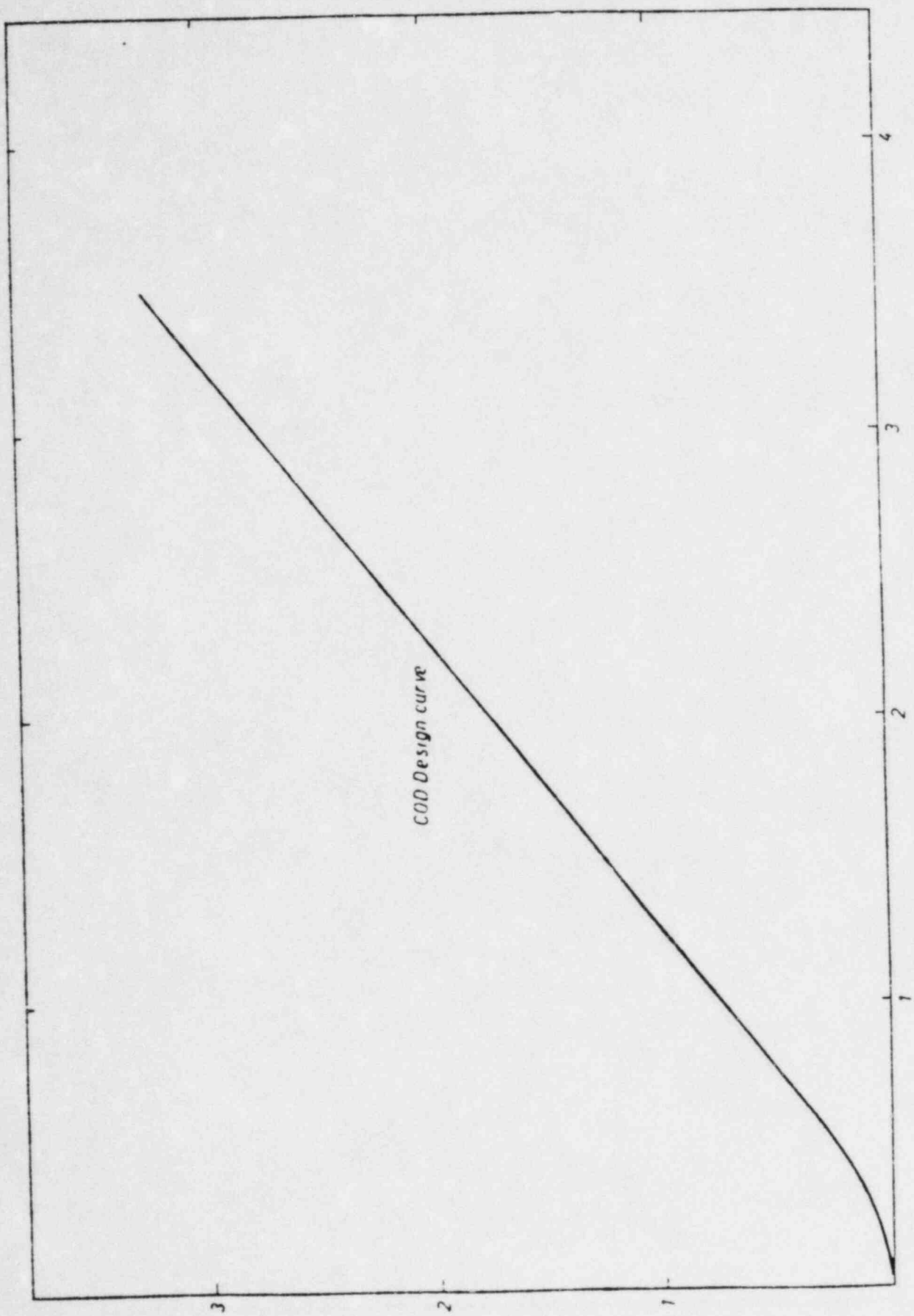

Figure 7-2 COD Design Curve (from Ref. 7-6)

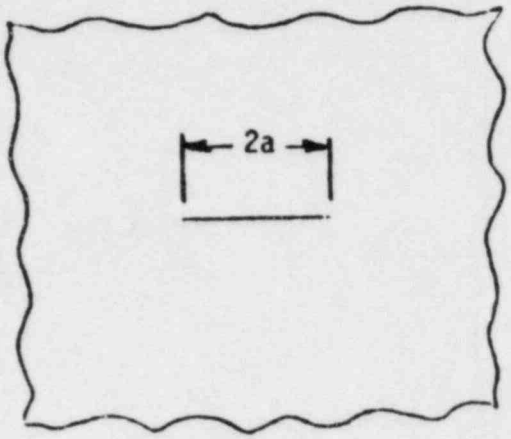

a) Through Flaw

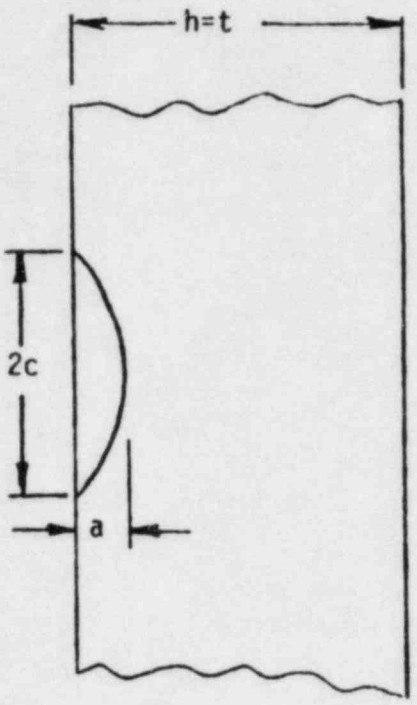

b) Surface Flaw

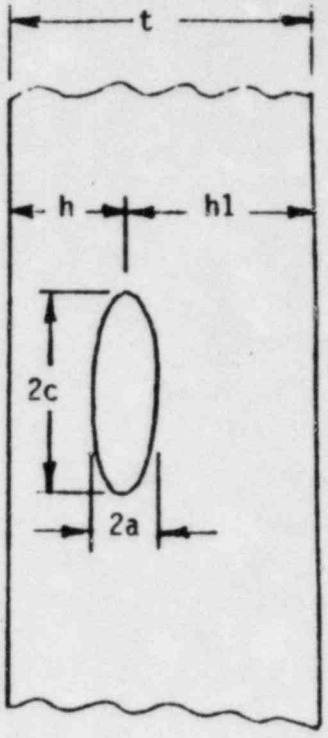

c) Buried Flaw

Figure 7-3 Defect Geometry

expression is:

$$K_I = \frac{M_T M_S}{\Phi_2} \sigma\sqrt{\pi a} \qquad (7.8)$$

where M_T is the magnification factor due to finite thickness effects, M_s is the free surface magnification factor, and Φ_2 is the elliptic integral of the second kind. It can be seen that

$$K_{\text{surface flaw}} = \frac{M_T M_S}{\Phi_2} K\left(\text{through-thickness flaw}\right) \qquad (7.9)$$

From this relationship, solving for an equivalent through-thickness crack size gives:

$$\frac{\bar{a}}{t} = \frac{a}{t}\left(\frac{M_T M_S}{\Phi_2}\right)^2 \qquad (7.10)$$

The values of $\frac{M_T M_S}{\Phi_2} = f\left(\frac{a}{t}, \frac{a}{2c}\right)$ were taken from a survey by Maddox (7-8), and are shown in figure 7-4.

It can be similarly shown that for a buried elliptical crack with the geometry shown in Figure 7-3c:

$$\frac{\bar{a}}{t} = \frac{a}{t}\left(\frac{M_o M_\pi}{\Phi_2}\right)^2 \qquad (7.11)$$

where M_o is the magnification factor at a point due to the nearest free surface and M_π is the magnification factor at that point due to the more remote free surface. These values were derived from the finite element

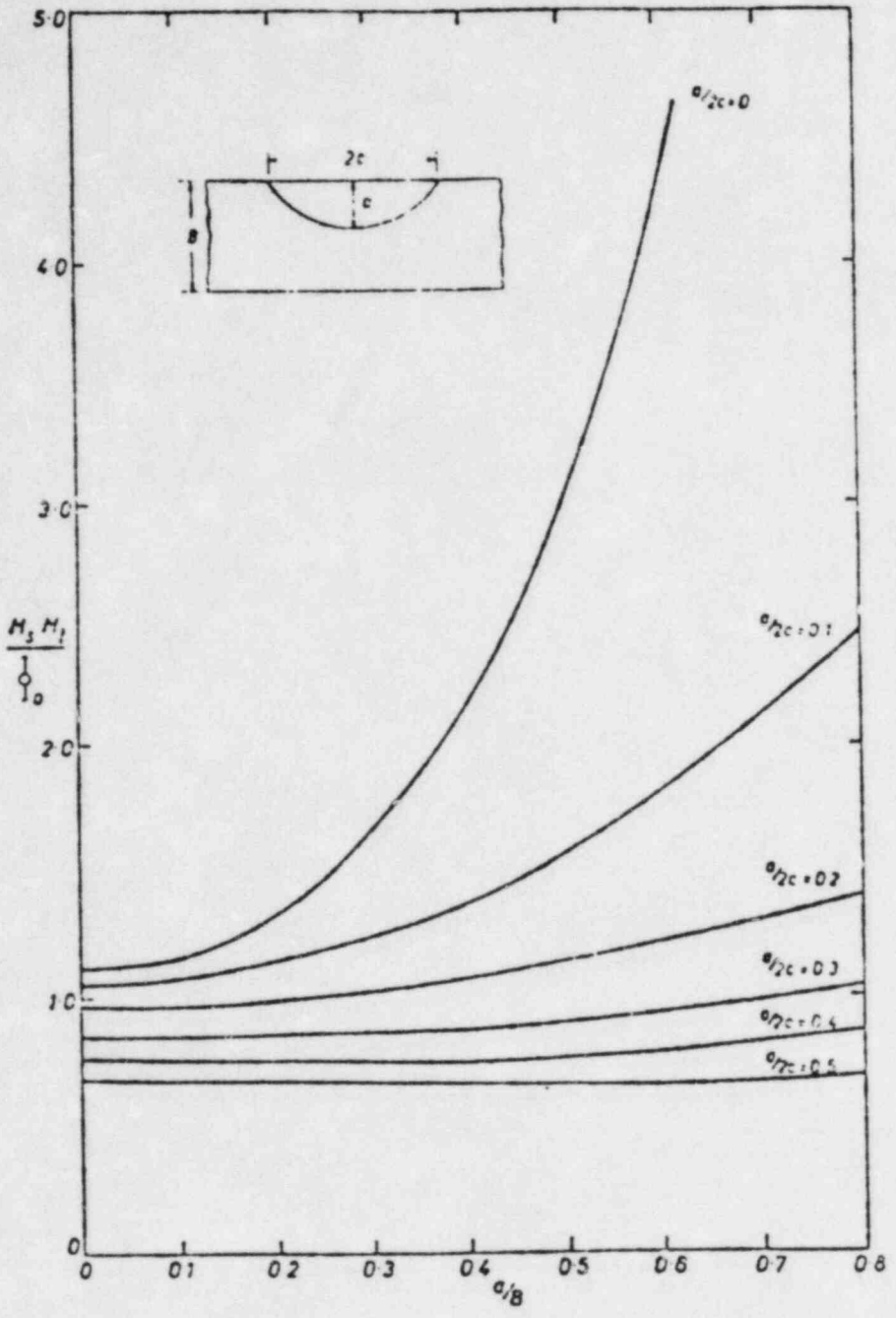

Figure 7-4 Variation of $(M_S M_T/\Phi)$ with Crack Depth for Various Shapes (from Ref. (7-7))

work by Shah and Kobayashi (7-9), and M_o and M_π are shown in Figures 7-5 and 7-6 respectively. The elliptic integral, ϕ_2, is plotted in Figure 7-7. For a/c = 0; $M_o M_\pi$ was derived from Fedderson's relationship (7-10):

$$M = \left(\sec \frac{\pi a}{t}\right)^{1/2}$$

Thus, combining the COD design curve with equations 7.6, 7.10, and 7.11, a relationship can be developed between allowable flaw size and allowable strain levels for each crack configuration. The Draft Standard contains criteria which require that when a crack tip approaches a free surface, the flaw should be reassessed as a surface-connected flaw (a buried flaw is recategorized as a surface flaw and a surface flaw is recategorized as a through-thickness flaw). The buried flaws present can be conservatively modeled as surface flaws and in the present case, only such surface flaws and through flaws have been considered.

The critical value for crack opening displacement was taken to be 0.023" as outlined in Section 5.4. The yield strain is assumed to be 0.2%. The calculated allowable flaw sizes for surface defects are shown in Figure 7-8 for 1.5 inch thick weldments.

The theoretical development used is valid to strain ratios (e/e_y) up to 2.5 but are plotted beyond that point to demonstrate that at flaw depths of approximately 10% of the wall, a very large margin to fracture exists. The results are shown for a variety of aspect ratios. For a/2c = 0.0, an infinitely long flaw is modeled. The theory provides a recategorization process at a depth of 50% of the wall thickness. The flaw should then be considered as a through-flaw.

Figure 7-9 shows the results of the elastic-plastic through-flaw analysis. The length of a critical flaw as a function of strain is given. For through- flaws, residual strains are not included.

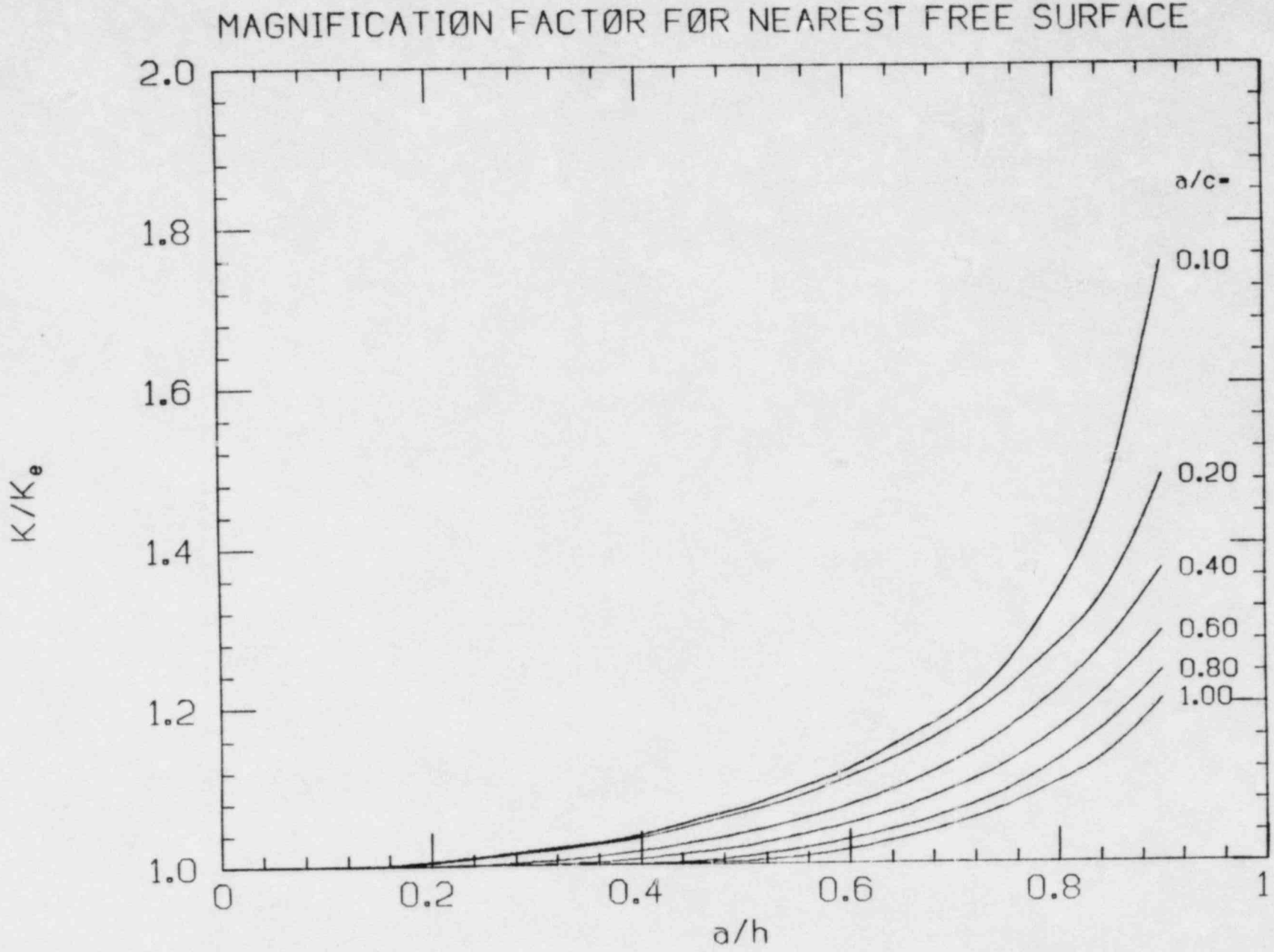

Figure 7-5

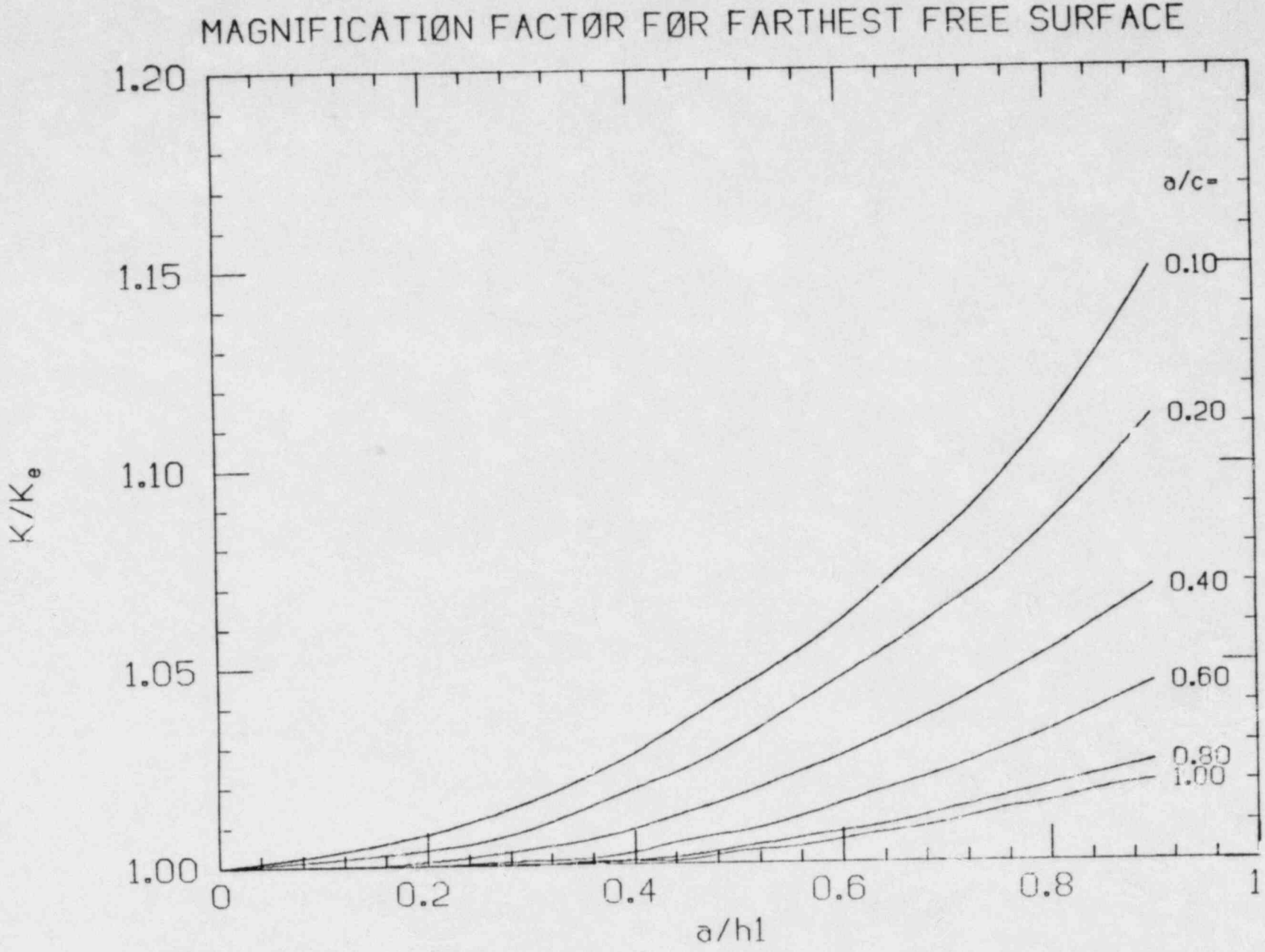
MAGNIFICATIØN FACTØR FØR FARTHEST FREE SURFACE
1.20
1.15
1.10
1.05
1.00
K/K$_e$
0
0.2
0.4
0.6
0.8
1
a/h1
a/c=
0.10
0.20
0.40
0.60
0.80
1.00

Figure 7-6

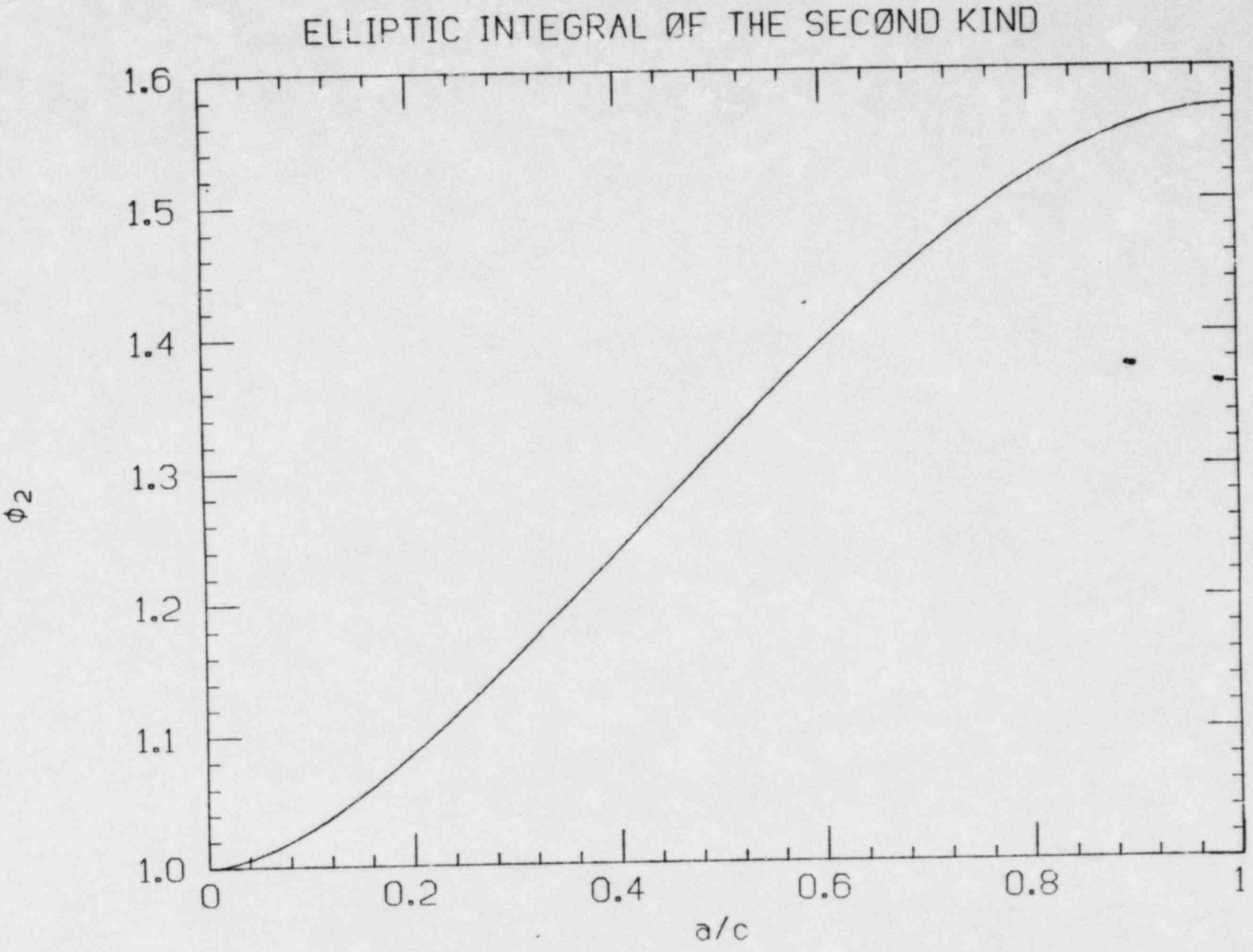
ELLIPTIC INTEGRAL ØF THE SECØND KIND
1.6
1.5
1.4
1.3
1.2
1.1
1.0
ϕ_2
0
0.2
0.4
0.6
0.8
1
a/c

Figure 7- 7

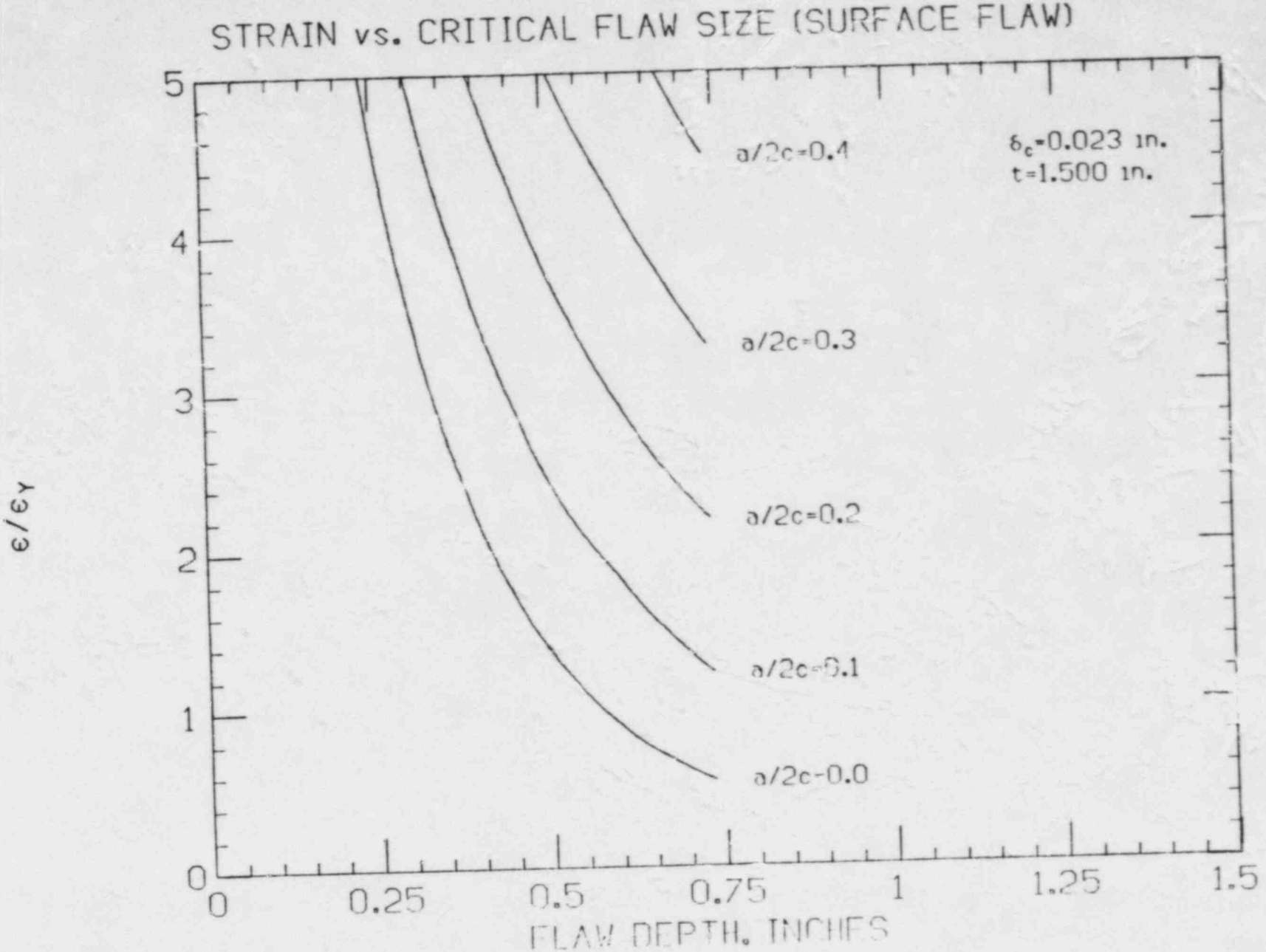

Figure 7-8 Strain versus critical flaw size for 1.5" thick weldments

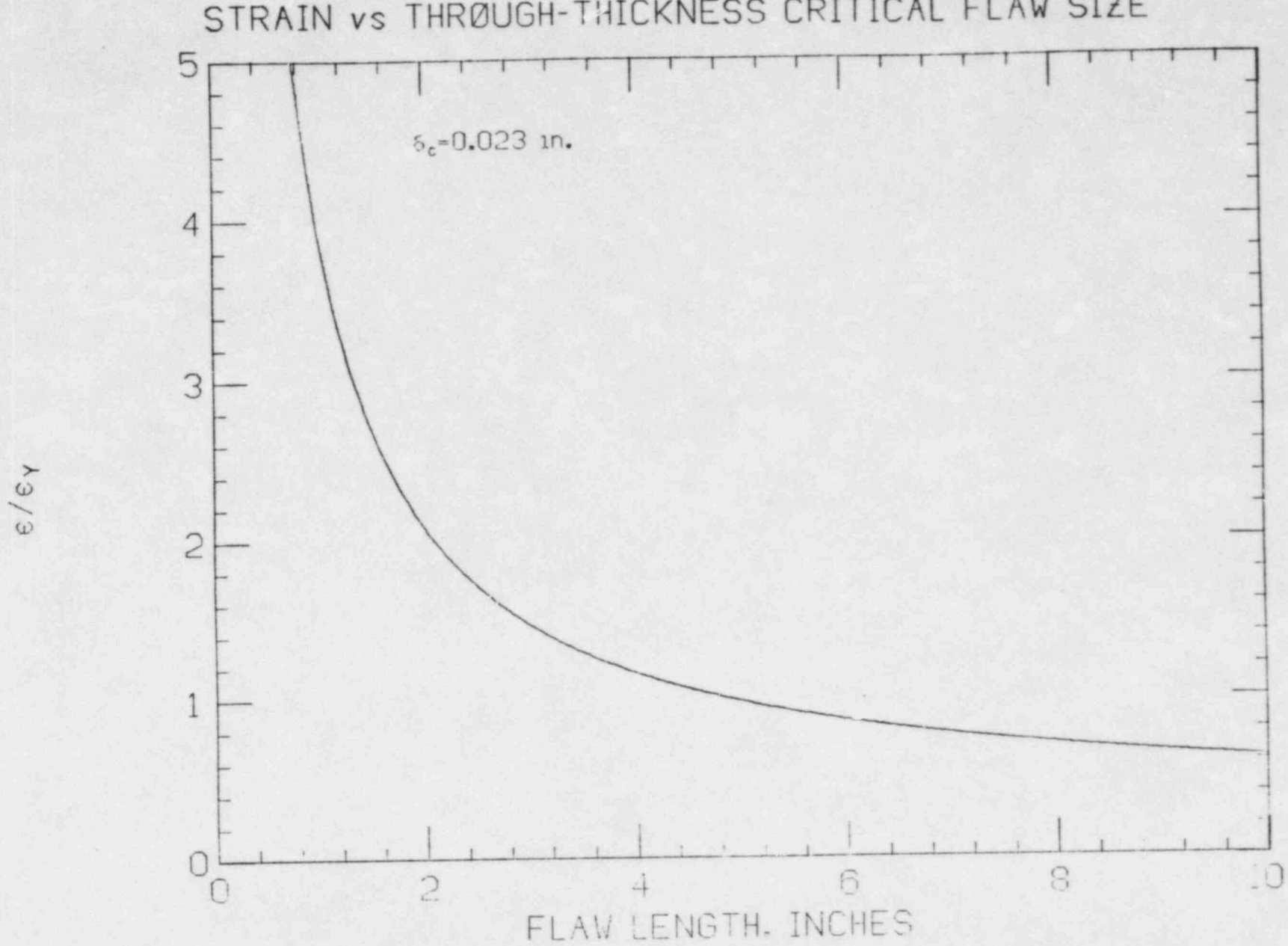

Figure 7-9 Strain versus through-thickness flaw (EPFM)

For the present case, the ratio of maximum applied strains to yield strain is approximately 0.5 so that long through-flaws are predicted prior to fracture by EPFM methods. Most relevant cases have lower strains and correspondingly larger predicted allowable flaw lengths.

Two notes are of interest here. First, the toughness used was taken from generic data and not plant specific information. Thus the flaw values should only be used to gauge the reasonableness of the LEFM approach as was their intent. Second, this EPFM approach has an inherent minimum factor of safety of 2 on flaw size.(7-11)

Section 7
REFERENCES

7-1 Chell, G.G., "Elastic-Plastic Fracture Mechanics," Central Electricity Research Laboratories, Report No. RD/L/R 200F, (August 1979).

7-2 American Welding Society, AWS A5.1-78, "Specification for Carbon Steel Covered Arc Welding Electrodes", 1978

7-3 British Standards Institution, "Draft Standard Rules for the Derivation of Acceptable Levels for Defects in Fusion Welded Joints", WEE/37, February, 1976.

7-4 Burdekin, F.M. and Dawes, M.G. "Practical Use of Linear Elastic and Yielding Fracture Mechanics with Particular Reference to Pressure Vessels", Institution of Mechanical Engineers C5/71.

7-5 Burdekin, F.M. and Stone, D.E.W., "The Crack Opening Displacement Approach to Fracture Mechanics in Yielding Materials", Journal of Strain Analysis, Vol. 1, No. 2, (1966), p. 194.

7-6 Harrison, J.D. et al, "The COD Approach and its Application to Welded Structures". The Welding Institute Research Report 55/1978/E, January (1978).

7-7 Dawes, M.G., "Fracture Control in High Yield Strength Weldments", Welding Journal Research Supplement, Vol. 53, (1974), p. 369s.

7-8 Maddox, S.J., "An Analysis of Fatigue Cracks in Fillet Welded Joints", International Journal of Fracture Mechanics, Vol. 11, No. 2, April (1975), pp. 221-243.

7-9 Shah, R.C. and Kobayashi, A.S., "Stress Intensity Factors for an Elliptical Crack Approaching the Surface in a Semi-Infinite Solid", International Journal of Fracture Mechanics, Vol. 9, No. 2, (1973) p. 133.

7-10 Fedderson, C.E., "Discussion to Plane Strain Fracture Toughness Testing". ASTM STP 410, (1967), p. 77.

7-11 Kamath, M.S., "The COD Design Curve: An Assessment of Validity Using Wide Plate Tests". The Welding Institute Report 71/1978/E, September, 1978.

Section 8
CONCLUSION AND SUMMARY

This report summarizes the results of an evaluation of the effect on structual integrity of several weld imperfections. These imperfections were assessed from indications in radiographs and have been analyzed in separate regions as follows:

- Inaccessible defects in weld seam 1-1 and 1-2
- Potentially rejectable inaccessible regions in weld 1-4
- Potentially rejectable inaccessible regions in welds 1-7 and 1-9

It has been found that assumed bounding defects of each category will not cause structural failure over the plant design lifetime. This analysis has included the effects of:

- Flaw growth by a fatigue mechanism
- Residual stresses
- Worst case applied stresses (steady state plus cyclic)
- Maximum defect sizes

Throughout the analyses, conservative estimates of input data have been used. These are summarized as follows:

- Methodologies. The LEFM method used has been shown to be

conservative in this analysis as compared with both elastic-plastic fracture mechanism and limit load methods. The LEFM calculated final flaw conditions do not account for the increased ductility that will be available at operating temperatures.

- Residual stresses. Bounding values from distributions published in the open literature for like weld details have been used.

- Flaw location in the through-thickness direction

- Flaw geometries. In all cases semi-elliptic surface flaws have been used to bound buried and near surface flaws. Many of the flaws thus bounded may be buried, in which case, substantially larger margins against failure occur than those listed.

- Crack growth rates. Upper bound crack growth rates for E7018 weld metal were developed and used to predict the amount of of crack growth.

- Choice of applied stresses. Bounding stress cases (including numbers of cycles) have been used.

- Material toughness. Material toughness values derived from COD data were shown to be conservative. In addition, data was collected at -20°F, which is much lower than the expected service temperature.

- Limit strength of the material. Values were estimated that result in conservative estimates of remaining ligament.

Appendix A
SUPPLEMENTAL TOUGHNESS DATA

APPENDIX A

CRACK OPENING DISPLACEMENT (COD) VALUES - E7018 WELD METAL

TEST TEMPERATURE (°F)	COD (in.)	DIAMETER (inches)	COMMENTS	REFERENCE
-20	.0182	5/32	Lincoln LH-70	I
	Ductile			
	Ductile			
-50	Ductile			
	Ductile			
-100	.0107			
-20	.0133	5/32	Lincoln LH-72	I
	.0192			
	Ductile			
-50	.0018			
	.0113			
-100	.0011			
+14	.0224	1/8, 5/32	Lincoln LH-72	I
	.0118			
	.0209			
			$10mm^2$ COD specimens for E7018 weld metal	II
-76	Tearing			
-76	>.030		$1\ in^2$ COD specimen. E7018 weld metal	

APPENDIX A
(Continued)

TEST TEMPERATURE (°F)	COD (in.)	DIAMETER	COMMENTS	REFERENCE
-94	10 values ranging from .008-.034 $\bar{x}$ = 20.00 s = 10.01		British equivalent to E7018	III
-40	22 values ranging from .016-.048 $\bar{x}$ = 34.45 s = 9.246		British equivalent to E7018	III
32	22 values ranging from .023-.052 $\bar{x}$ = 39.68 s = 7.305		British equivalent to E7018	III

APPENDIX A

REFERENCE LIST FOR FRACTURE TOUGHNESS DATA - E7018

I. Personal correspondence between W. McNaughton (Aptech Engineering Services) and R.C. Shutt (The Lincoln Electric Company), Dated May 22, 1979.

II. Dawes, M.G., "Designing to Avoid Brittle Fracture in Weld Metal," Metal Construction and British Welding Journal (February 1970), Pp. 55-59.

III. Tait, P. and D.M. Haddrill, "Fracture Toughness of Some Mild Steel Manual Metal-Arc Weld Deposits," Welding and Metal Fabrication (September 1970), Pp. 370-375.

Appendix B

BACKGROUND INFORMATION ABOUT DIGITAL IMAGING TECHNIQUES

APTECH imaging DIGITAL IMAGING SYSTEMS

795 SAN ANTONIO ROAD • PALO ALTO • CALIFORNIA 94303 (415) 858 • 2866

INSPECTION SIGNAL ENHANCEMENT SERVICES FOR THE NUCLEAR POWER INDUSTRY

Aptech Imaging, Inc., has developed unique digital signal enhancement schemes which are applicable to a wide range of inspection signals. Three particular applications of this technology have been developed as follows:

Enhancement of existing inspection information, such as x-rays, radiographs, or videotapes.

Real-time x-ray imaging systems or filmless radiography.

Records management to store and retrieve in digital format, radiographs, engineering drawings, etc.

These enhancement techniques have already had wide application in the nuclear power industry to aid resolution and interpretation of inspection signals. We have outlined below some relevant experience in the nuclear power industry.

CLIENT	SERVICES PROVIDED
Southern California Edison San Onofre Generating Station Unit I	Enhancement of indications in radiographs of welds in main steamlines
Boston Edison Company Pilgrim I	Enhancement of images from underwater television cameras of core spray sparger. This work was performed by enhancing existing video tape recorded in 1980. We performed on-site real-time enhancement in conjunction with the inspection at the 1981 outage.
Gilbert Commonwealth Asspciates/ Cleveland Illuminating Company Perry Nuclear	Enhancement and interpretation of radiographs of containment welds.
Rolls Royce Nuclear Ltd	Enhancement and interpretation of old radiographs.
General Electric Company	Enhancement and restoration of out-of-specification radiographs for cast nuclear valve bodies.

Nuclear Regulatory Commission	Enhancement of radiographs of stress corrosion cracks adjacent to welds in Type 304 stainless steel.
Bechtel Power Corporation	Demonstration of digital records management system to store and retrieve radiographs and engineering drawings.
Battelle, North West	Demonstration of enhancement techniques for underwater viewing of reactor internals.
Consolidated Edison Company	Radiographic enhancement for defects and restoration of old radiographs.
General Electric Company	Enhancement and interpretation of defects in radiographs of nuclear plant valve bodies.
GPU Nuclear	Enhancement of video tape inspection records of core spray sparger.
	Enhancement of video tape inspection records of core spray riser piping and reducer.
	On-site real time enhancement of video signals from core spray sparger and annulus inspection.
Northern States Power	Enhancement of radiographs of stress corrosion cracks in primary piping.
Power Authority, State of New York	Enhancement of original fabrication radiographs from steam generator closure weld.
Bechtel Power Corporation South Texas Project	Determination of defect dimensions (length and depth) in emergency cooling water lines.
Duke Power Company	Enhancement of radiographs from pipe to valve welds.
North East Utilities	Enhancement of piping radiographs from Millstone III.

Further details about these services and individual utility contacts can be provided to you on request.

PAPER NO 28 CONFERENCE Fracture Toughness Testing — Methods, Interpretation & Application
AUTHOR(S) G.R.Egan, M.F.Elgart & A.A.Smith
As received late type script

IMPROVED RADIOGRAPHIC FLAW SIZING BY DIGITAL IMAGE PROCESSING

G. R. Egan,* M. F. Elgart,** and A. A. Smith***

1.0 SYNOPSIS

This paper describes the calibration and application of a digital image processing method to determine the depth of indications seen on radiographs. The image of the radiograph is digitized and then computer manipulated to provide accurate measures of film density. Indications on the radiograph can then be interrogated to determine their extent in the through thickness direction. By comparing numerical measurements of density of indications with known density changes from image quality indicator wires or the plate thickness, the depth of indications can be determined.

A calibration procedure is also described wherein known defects were introduced into a steel sample which was then radiographed. A comparison of the digital processing size estimates and the actual dimensions of the defects shows excellent correspondence. An example of the application of this technique to lack of root fusion defects is also described.

*APTECH Engineering Services, Inc.
**Aptech Imaging, Inc.
*** Consulting Engineer

2.0 INTRODUCTION

Fracture mechanics principles have been used to characterize a wide range of failure mechanisms including brittle fracture, ductile fracture, fatigue, stress corrosion cracking, and also weld cracking phenomena. The analysis required to characterize any of these crack extension mechanisms is based on determining a material property (e.g., toughness in the case of fracture problems), the acting stresses that can cause crack extension, and calculating the critical flaw size for crack initiation or continued crack propagation. In any of the analysis methods that have been developed there are uncertainties in the input data that are used. For example, in the very simple case of assessing the critical flaw size to cause brittle fracture, scatter in data of K_{IC} tests, uncertainty in the definition of stresses including residual stresses and the errors associated with flaw sizing techniques mean that when critical flaw sizes are calculated, margins of safety must be established before the results can be applied.

Since, in most cases, there are insufficient data to perform a full probabilistic analysis of the problem, it is necessary to choose bounding values of the input data to fracture mechanics equations so that the resulting calculated value of critical stress or critical flaw size is regarded as a conservative estimate. Pursuing this procedure to its logical conclusion often results in such pessimistic predictions that currently operating equipment is deemed to be in jeopardy from some predicted failure mechanism (1). It may well be the case that operating limits are so restricted that major economic penalties are incurred by performing so-called "conservative analyses." One answer to this dilemma is to perform the complete probabilistic analysis to establish the probability of failure by the mechanism that is described by the deterministic fracture mechanics equations (2). Having derived this number, however, there is usually uncertainty in establishing the significance of such numbers (3) and comparisons of risk between different events can be made to judge the comparative significance of an outcome.

By looking at uncertainty in the input parameters, it is possible to establish a ranking of importance of input variables to any fracture mechanics analysis. For example, by the very nature of the equations that describe the interrelated

variables, we are able to establish a ranking in order of the importance of particular input parameters. With this ranking, we can then concentrate on refining methods for decreasing the uncertainty in any set of input data.

The importance of establishing the initial flaw size can be determined by studying the equations which describe some of the fundamental failure mechanisms. Table 1 outlines the relationship between calculated critical flaw size and the measured flaw size for three different failure mechanisms--fracture, high cycle fatigue, and stress corrosion cracking in sensitized Type 304 steel (4). It can be seen that the importance of flaw size dimensioning increases as the exponent of K or ΔK in the equation that describes the failure phenomenon. This has also led to the establishment of the half life concept for both fatigue and stress corrosion cracking (5).

In this paper, we concentrate on developing methods to improve sizing of defects discovered by either x-ray or radiographic techniques. We anticipate that this work will lead to better and more reliable methods of flaw sizing.

Although much research is currently being undertaken to improve the reliability of inspection systems, it is clear that a key element that contributes to the uncertainty is the presence of a human interpreting and recording information. The work that we describe following is aimed, in the long term, at providing automatic pattern recognition systems for flaw detection and sizing.

Table 1

IMPORTANCE OF FLAW SIZE IN FRACTURE MECHANICS ANALYSIS

FAILURE MECHANISM	GOVERNING EQUATION	FLAW SIZE DEPENDENCE
Brittle Fracture	$\sigma_c \propto \frac{K_1}{\sqrt{\pi a}}$	$a^{-\frac{1}{2}}$
Fatigue	$N \propto \frac{1}{\Delta\sigma^m}\left[1 - \left(\frac{a_i}{a_f}\right)^{\frac{m-2}{2}}\right]$	$a^{\frac{1}{2}*}$
Stress Corrosion Cracking of Sensitized 304	$T \propto \sigma_{max}^{-m} a_i^{\frac{m-2}{2}}$	a^{-3**}

*For m = 3
**For m = 8

3.0 DIGITAL IMAGE PROCESSING TECHNIQUES

3.1 Background

The digital image processing techniques that we have developed are described in detail elsewhere, however, a short summary of the basic background technology will be provided here (6). A diagram of the equipment that is used to capture images in digital format is shown in Fig. 1. The image collection system (i.e., a television camera) can deal with signals from x-rays, radiographs, pictures, and printed pages. Once the information is digitized and stored in the computer, manipulation by mathematical methods of analysis can be performed to provide images that can be interpreted by the non-expert. The APTECH system shown in Fig. 1 outputs information to a television monitor from which hard copy can be obtained by normal photographic means. In addition, copy can be provided on either magnetic tape, video tape, or video disc.

3.2 Treatment of Radiographs

The primary advantage of radiography as a nondestructive testing technique is associated with the fact that an image is involved. The use of an image enables both expert and non-expert to interpret effectively the meaning of the test results. However, because of his experience, the expert radiographer will usually extract more information from an image than a non-expert will. The amount of discernible information is unfortunately biologically limited. Although film contains sufficient information to detect density differences of 0.05% to 0.1%, the human eye can only resolve grey levels which differ by at least 1.5%. Therefore, the film has captured much more information than the eye can extract.

Additionally, the eye discerns a boundary or edge condition only when two adjoining areas of an image differ by more than 15% in density. The full range of film density information can be made available to the observer by use of digital techniques of analysis. Small density differences not discernible to the unaided eye can be made visible on a television monitor by expanding a small density range on film to the full white to black grey level information. Then

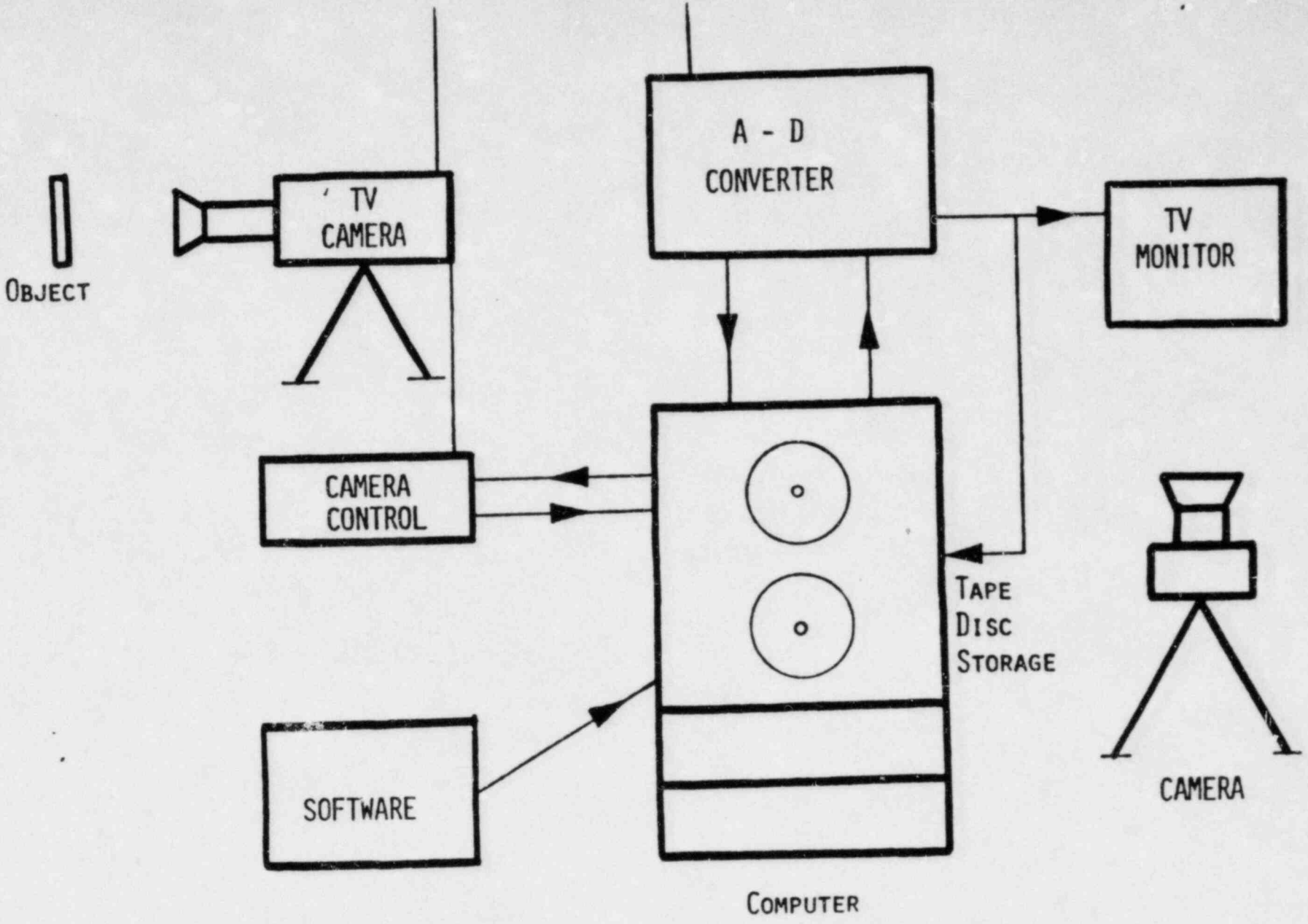

Figure 1 - Aptech Imaging System.

since the image is in discrete digital form, mathematical methods can be directly applied to provide image enhancement. Images are currently captured using a 512 x 512 matrix, and each pixel in this matrix contains grey level information. Grey level information or radiographic density is provided on a scale from 0 to approximately 4000.

3.3 Procedures for Depth Measurement of Indications

Since the computer can discern density differences from white to black, on a grey level scale of 0 to 4000, the sensitivity on depth measurement in a full grey scale is 1/4000 of the depth of the piece being examined. Furthermore, for defects that lie normal to the plane of the radiograph, it is possible to establish a density or defect size profile using information derived from image quality indicators or the plate thickness. For example, since the computer provides such a sensitive measure of density, it is possible to calibrate a radiograph by using density changes associated with image quality indicators. Details of this procedure are outlined later.

In addition, for dimensional verification, for establishing the dimensions of radiographic indications in the plane of the radiograph, it is possible to perform automatic integration schemes that will yield defect length and width. The sensitivity of these measurements is 1/512 of the extent of the image being processed. Since mathematical magnification models are available, it is possible to develop the required sensitivity in the length and width directions. An example of dimensional verification by computer is shown in Fig. 2.

The foregoing description leads to the natural conclusion that we are able to plot out in three dimensions, defect profiles. From a single radiograph, it is possible to do this; however, one important piece of information is missing and that is the location of the indication within the thickness of the part being examined. The procedure has certain limitations related to the eccentricity of buried defects, however, for surface connected defects, the procedure can be used in a straight forward manner. Some comments are made later on how the procedure may be changed to establish positional information relative to the two free surfaces of the parts being examined.

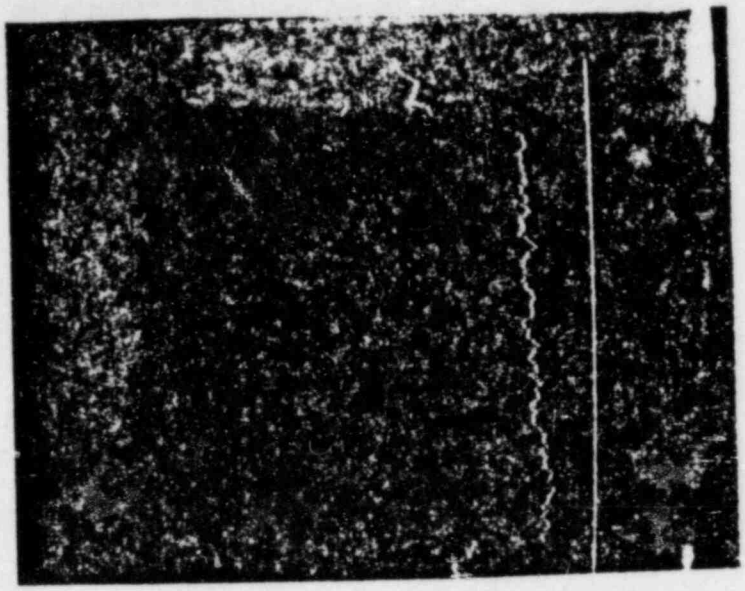

2a. Digital Information Plotted to Define Edge.

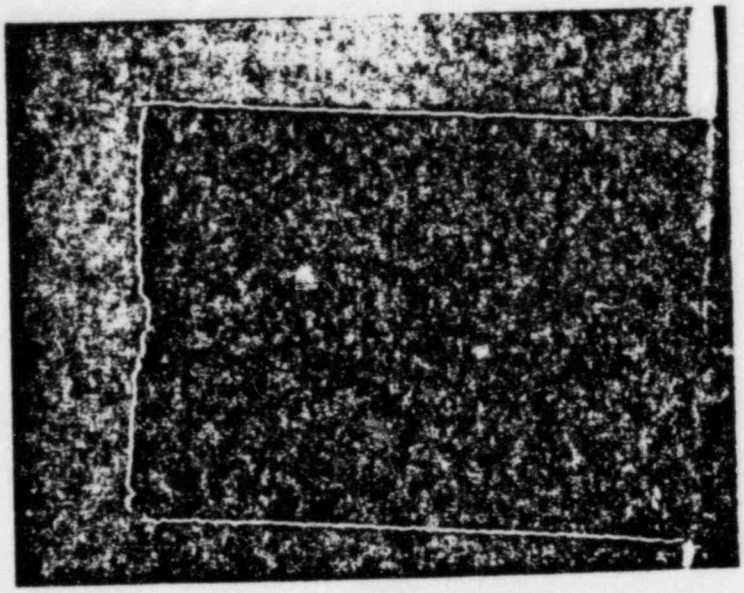

2b. Dimensioning by Computer.

Figure 2 - Example of Dimensioning by Computer.

3.4 Calibration

To determine that the procedure does provide accurate measures of defect depth into a plate from a single radiograph, we have performed a calibration procedure using blocks containing defects of known dimensions. Details of the calibration blocks are shown in Fig. 3. For convenience, we shot the calibration blocks in real time and captured the information on videotape which was subsequently digitized and processed. The image could also have been collected on film.

Once the image had been collected on videotape, the information was presented to the computer in digital format. We were then able to establish measures of defect height through the thickness for the range of defects contained in the blocks (Fig. 4). The defects consisted of machined notches and drilled holes, and these were also measured using gauge blocks. A comparison of the two methods of measurement is shown in Table 2. It can be seen that a small uncertainty still exists in the dimensioning of defects by this method, but it is significant improvement on existing methods of determining size information by nondestructive means.

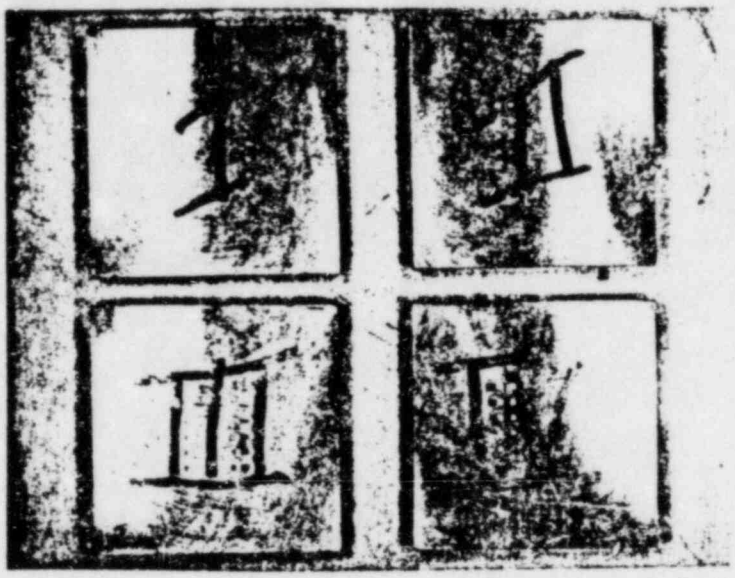

Figure 3 - Calibration Blocks.

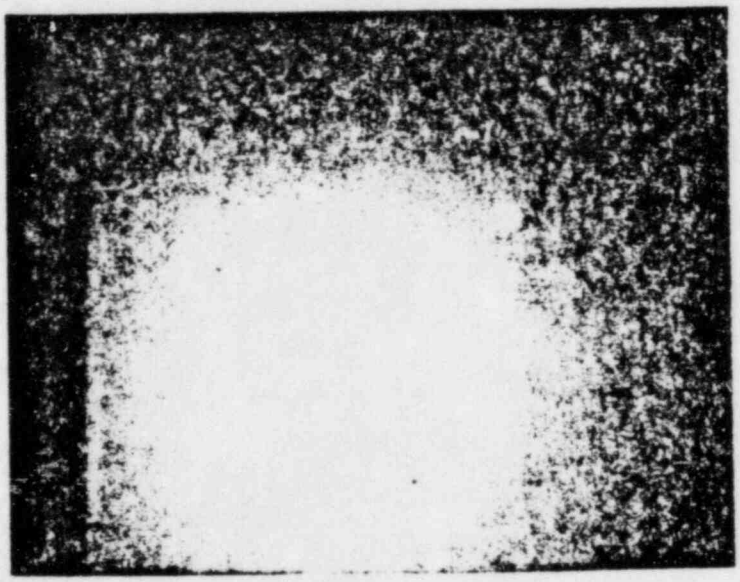

Figure 4 - Photograph of TV Monitor Displayed Image of Real Time X-Ray of Block IV.

Table 2

RESULTS OF CALIBRATION - BLOCK 4

Defect	Digital Information Full Plate	Digital Information Defect	Estimated Depth (inch)	Measured Depth (inch)
4S1	2550 2775	3390	0.107	0.110
4S2	2775 2900	3380	0.800	0.075
4S3	2900 2925	3370	0.068	0.060
4H1	2200 2200 2200 2200	3260	0.162	0.113
4H2	2350 2350 2250 2200 2335	3050	0.125	0.098
4H3	2400 2400 2350	2870	0.086	0.067

4.0 APPLICATIONS

In this Section, we outline a specific application of this technique to indications derived from radiographs of offshore platform welds. In each case, we have determined a calibration coefficient from the image quality indicator and the part thickness and used this to establish the through thickness extent of indications in the radiograph. These dimensions can then be compared with fracture mechanics calculations to support continued operation of these structures.

4.1 Offshore Pipeline Welds

In this particular example, we were supplied with radiographs of welds from the main legs of fixed platforms located in relatively shallow water (i.e., less than 100 feet). The radiographs were generally of poor quality and out of focus because of the large object to film distance. We processed the radiographs by applying an artificial focus procedure which essentially consists of squeezing the digital information down until the picture becomes focused. The results of this procedure are shown in Fig. 5. After this procedure was completed, we then interrogated the image quality indicator wires to establish a unique calibration for each radiograph. Having done this, we then established the depth of indications that were apparent in the root of the welds. These were surface connected defects so that the calibration procedure was straight forward, and the missing information for through thickness position was not necessary. An example of the procedure used is shown in Fig. 6.

From Fig. 6, it can be seen that not only can depth information be established, but the procedure also provides information about the type of indication (i.e., rounded or linear). The technique has also been used for defect identification.

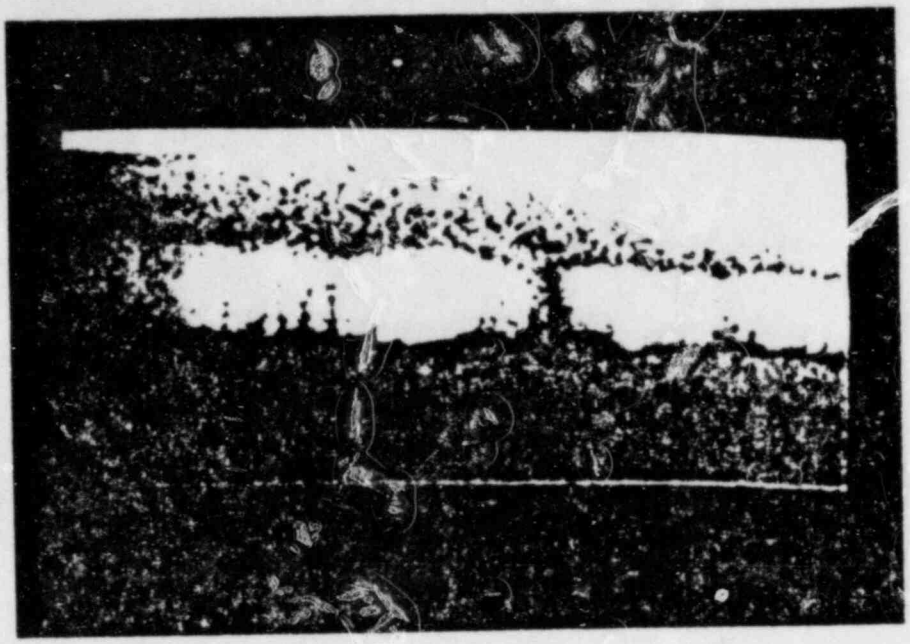

Figure 5 - Root Pass of Weld in Offshore Platform.

Figure 6 - Example of Digital Screening for Defect Depth and Dimensions.

5.0 CONCLUDING REMARKS

It would be unrealistic to conclude without a few cautionary comments. First, the technique that we have developed can only be used on images that have not been enhanced using non-linear transforms. Obviously, in such enhancements, where particular parts of the grey scale are compressed, a calibration on one part of the radiograph would not apply at other locations on the radiograph. Second, where the indications are smaller than one pixel (1/512 of the image), unique depth information cannot be determined. This is not really a practical limitation because it is possible to capture a smaller part of the radiograph.

In addition, from a single radiograph we cannot determine the location of the indication in the through thickness direction. It is necessary to take one other shot at an angle to be able to reconstruct all of the positional information.

Even in spite of these limitations, we have found that for surface connected defects there is a need for an accurate method of estimating depth of indications. The work is continuing with the objective of developing an automated process for providing defect dimensions and positions.

REFERENCES

1. Snaider, R. P., J. M. Hodge, H. A. Levin, and J. J. Zudans, "Potential for Low Fracture Toughness and Lamellar Tearing on PWR Steam Generator and Reactor Coolant Pump Supports. Resolution of Technical Activity A-12," NUREG-0577 for Comment, Office of Nuclear Reactor Regulation, U.S. Nuclear Regulatory Commission (October 1979).

2. Thomas, J. M. and D. C. Peters, "Probabilistic Decision Model for Structures Subjected to Crack Growth and Fracture," ASME Winter Annual Meeting, San Francisco (1978).

3. C. Starr, "Benefit-Cost Studies in Socio-Technical Systems," Colloquium on Benefit-Risk Relationships for Decision Making, Washington, D.C. (April 1971).

4. Egan, G. R. and R. C. Cipolla, "Stress Corrosion Crack Growth and Fracture Predictions for BWR Piping," ASME, New York (1978).

5. Hayes, D. J., "Fracture Mechanics Based Fatigue Assessment of Tubular Joints. Review of Potential Applications," AES 81-01-45, Shell Oil Company (January 1981).

6. Elgart, M. F. and R. H. Richman, "Real Time Digital Techniques for Radiography," Proceedings of Workshop on Nondestructive Evaluation of Turbines and Generators, EPRI WS 80-133 (July 1981).

Appendix C

DETAILS OF THE FLAW CHARACTERIZATION WORK

SUMMARY OF RADIOGRAPHS REVIEWED
INACCESSIBLE WELDS

JOINT	STATION	DEFECT	LENGTH (Max)	DEPTH (Max)
Unit 1				
1-1 (21-22)	4-5	Elongated Slag	0.75"	5.8%
1-1 (21-22)	5-6	LOF	4.0"	11.0%
1-1 (21-22)	11-12	LOF	1.0"	11.4%
1-1 (21-22)	12-13	LOF	0.3"	10.7%
1-1 (24-25)	9-10	Elongated Slag	0.5"	6.0%
1-1 (24-25)	16-17	LOF	0.63"	13.3%
1-1 (25-26)	10-11	LOF	0.4"	11.1%
1-1 (26-27)	9-10	LOF	0.75"	12. %
1-1 (27-28)	4-5	LOF	0.2"	8.8%
1-1 (28-29)	3-4	LOF	0.6"	3.9%
1-1 (28-29)	4-5	Slag	4.5"	8.8%
1-1 (28-29)	5-6	Elongated Slag	0.32"	8.7%
1-1 (28-29)	18-19	LOF	0.5"	13.6%
1-1 (29-30)	X-17	LOF	0.5"	12.5%
1-1 (30-31)	8-9	Elongated Slag	0.75"	5.4%
1-1 (31-32)	11-12	Elongated Slag	1.25"	10.0%
1-1 (32-33)	2-X	Elongated Slag	1.0"	11.3%
1-1 (33-34)	24-25	No Defects Observed		
1-1 (34-35)	17-18	Crack/Pore	0.5"	8.8%
1-1 (35-19)	1-2	LOF	0.5"	1.7%
1-1 (35-19)	6-7	Isolated Slag	0.19"	5.3%
1-4 (79-80)	11-12	Slag	0.7"	4.5%
Unit 2				
2-1 (19-20)	1-2	Slag/LOF	1.0"	shallow
2-1 (19-20)	3-4	Pore/LOF	0.62"	9.0%
2-1 (19-20)	4-5	Slag/Pore/LOF	0.25"	5.0%
2-1 (19-20)	12-13	Slag	0.75"	shallow
2-1 (19-20)	15-16 R1	Slag/Pore	0.4"	shallow
2-1 (19-20)	17-18 R1	Slag/LOF	0.4"	shallow
2-1 (19-20)	18-19	Slag/LOF	0.75"	4.0%

JOINT	STATION	DEFECT	LENGTH (Max)	DEPTH (Max)
2-1 (20-21)	10-11	Slag	0.5"	shallow
2-1 (20-21)	11-12	Slag/LOF	0.62"	6.2%
2-1 (20-21)	12-13	LOF	0.5"	shallow
2-1 (20-21)	14-15	Slag/LOF	0.4"	very shallow
2-1 (21-22)	4-5	Slag	0.5"	shallow
2-1 (21-22)	5-6	Slag/LOF	0.5"	7.4%
2-1 (22-23)	11-12	LOF	0.4"	shallow
2-1 (24-25)	7-8	Slag/LOF	0.5"	5.3%
2-1 (27-28)	0-1 R3	LOF	0.31"	shallow
2-1 (27-28)	1-2	Slag/LOF	0.62"	shallow
2-1 (27-28)	11-12	Slag/LOF	0.4"	rounded
2-1 (27-28)	13-14	LOF	0.5"	3.0%
2-1 (27-28)	16-17	LOF	0.6"	shallow
2-1 (27-28)	19-20	Slag/Pore	0.4"	rounded
2-1 (28-29)	12-13	Slag	0.75"	shallow
2-1 (28-29)	13-14	Slag	0.5"	shallow
2-1 (28-29)	24-25	Slag	0.62"	6.0%
2-1 (28-29)	25-0	Slag/Pore	0.62"	7.6%
2-1 (30-31)	0-x	Slag	0.5"	shallow
2-1 (30-31)	6-7	Slag/LOF	0.4"	shallow
2-1 (30-31)	11-12	Slag	0.19"	very shallow
2-1 (30-31)	12-13	Slag/LOF	0.5"	7.3%
2-1 (30-31)	13-14	Slag/LOF	0.5"	very shallow
2-1 (32-33)	8-9	Slag	0.25"	very shallow
2-1 (32-33)	10-11 R2	Slag	0.4"	very shallow
2-1 (32-33)	11-12	Slag/LOF	0.4"	8.0%
2-1 (32-33)	16-17	Slag	0.4"	10.0%
2-1 (32-33)	19-20	Slag/LOF	0.5"	7.7%
2-1 (32-33)	23-24	Pore/LOF	0.5", 0.06"	5.7%, 9.0%
2-1 (33-34)	7-8 R1	Slag/LOF	0.5"	12.5%
2-1 (35-19)	0-1	Slag	0.19"	shallow
2-1 (35-19)	1-2	Slag/LOF	0.19"	7.1%
2-1 (35-19)	10-11	Slag/LOF	0.25"	3.8%
2-1 (35-39)	14-15 R1	Undercut/Slag	1.125"	14.3%
2-1 (35-39)	15-16	Slag	0.5"	10.7%
2-1 (35-39)	20-0	LOF	0.5"	7.7%

Appendix D

CONTROLLED DOCUMENTS

APTECH ENGINEERING SERVICES DOCUMENT LOG

CONTROLLED DOCUMENT NUMBER	ITEM	
4	(AES-8110276) Volume 1 of 1 Containment Horizontal Stiffener Ring Flanges for rings 1-4 including CMTR's.	
7	(AES-8110276) Volume 1 of 1 Containment Horizontal Stiffener Ring Flanges for rings 5 and 6, including CMTR's.	
125	Letter PY-CEI/GAI-5519 dated 11-15-82 from W.T. Melia to R. Alley.	
126	NNIC letter dated October 26, 1982 to R.W. Alley from B.R. Cofer on subject of Perry Nuclear Power plant containment vessel analysis of weld 1-1.	
127	Certified material test reports of weld 1-1 between vertical welds 21-22.	
128	R. Dail preliminary report to R.W. Alley dated November 16, 1982 on limited review of containment vessel radiographs.	
129	Longitudinal stresses weld 1-1 showing thermal, hydrostatic, design pressure, dead load, SRV, OBE and SSE stresses.	Rev. 0
130	Letter PY-STR-1555 information, dated November 29, 1982, from R.W. Alley to W. McNaughton, including Rev. 1 of stresses included in CD-129.	
131	Letter dated 11-5-81 from B.R. Cofer, NNIC to R.W. Alley, GAI on subject of containment Vessel Analysis of Weld 1-1 Indication	
132	NNIC letter dated 9-24-82 on preliminary summary containment vessel embedment analysis - Figures 1 and 3.	
133	UT reports - inaccessible shell joints.	
134	Letter to J. Keppler from D. Davidson dated 9-30-82.	
135	Letter to R. Dail from W. McNaughton results of enhancement of radiographs 1-50 A/B (1-2), 1-1 (17-18), 1-1 (24-25).	
136	Letter to W. McNaughton from R.W. Alley transmitting radiographs 1-1 (24-25), 9-10 and 1-2 (45-46), 14-15.	

CONTROLLED DOCUMENT NUMBER	ITEM
137	Letter report dated December 7, 1983, W. McNaughton to P. Gudikunst preliminary results of inaccessible defect evaluation, weld 1-1.
138	BIGIF computer runs
139	Letter from R.W. Alley to W. McNaughton PY-STR-1587, February 16, 1983
	Attachment 1: Memo R. Dail to R. Alley Unit 1 containment radiographs
	Attachment 2: Stresses in Joints 2-6.
	Attachment 3: Memorandum E.M. Horeth to B.R. Cofer, December 7, 1982
	Attachment 4: Memorandum B.R. Cofer to M. Lastovka, December 17, 1982
	Attachment 5: Memorandum R.L. Dail to R. Alley January 4, 1983 "Review of NNIC Evaluations of Indications in Containment vessel circumferential welds 1-4.
	Attachment 6: Letter B.R. Cofer to R.W. Alley, February 3, 1983 "Data for Analysis of Welds 1-7 and 1-9.
140	Receipt of Design Materials letter from W. McNaughton to P. Gudikunst, December 20, 1982.
141	Letter from W. McNaughton to K. Nebb (site) returning radiographs dated 3-11-83.
142	Acknowledgement of receipt of radiographs listed in CD-141 (from K. Webb)
143	Letter from K. Webb (site) sending (29) radiographs with acknowledgement 3-23-83.
144	Letter from K. Webb (site) sending (15) radiographs with acknowledgement 3-24-83.
145	Letter from R. Alley to W. McNaughton summarizing radiographs sent and stresses which correspond. PY-STR-1607 3-31-83.

CONTROLLED DOCUMENT NUMBER	ITEM
146	Letter from K. Webb (site) to W. McNaughton sending 6 radiographs 4-4-83.
147	Letter from W. McNaughton to R. Alley April 19, 1983 "Aptech Evaluation of 4 shell courses defects - background information".
148	Summary of radiographs reviewed consisting of notes and measurements.
149	Documentation of locations on each radiograph of CD-148 as to depth measurement location.
150	Videotape with balance of Gilbert enhancement.
151	Stress calculations - load combinations as taken from CD-139 and checked.
152	Developed integrated stresses - service and residual stresses.
153	Limit load analysis.
154	BIGIF runs used in final report - 1H1, 1H2, 1H5, 1H6, 6H1, 6H2, 6H3, 6H4, 8H1, 8H2